nature protocols

https://doi.org/10.1038/s41596-024-01106-8

Protocol

Check for updates

A multifunctional sensor for cell traction force, matrix remodeling and biomechanical assays in self-assembled 3D tissues in vitro

Bashar Emon[1], Md Saddam Hossain Joy[1], William C. Drennan[1] & M. Taher A. Saif[1,2]

Abstract

Cell–matrix interactions, mediated by cellular force and matrix remodeling, result in dynamic reciprocity that drives numerous biological processes and disease progression. Currently, there is no available method for directly quantifying cell traction force and matrix remodeling in three-dimensional matrices as a function of time. To address this long-standing need, we developed a high-resolution microfabricated device that enables longitudinal measurement of cell force, matrix stiffness and the application of mechanical stimulation (tension or compression) to cells. Here a specimen comprising of cells and matrix self-assembles and self-integrates with the sensor. With primary fibroblasts, cancer cells and neurons we have demonstrated the feasibility of the sensor by measuring single or multiple cell force with a resolution of 1 nN and changes in tissue stiffness due to matrix remodeling by the cells. The sensor can also potentially be translated into a high-throughput system for clinical assays such as patient-specific drug and phenotypic screening. We present the detailed protocol for manufacturing the sensors, preparing experimental setup, developing assays with different tissues and for imaging and analyzing the data. Apart from microfabrication of the molds in a cleanroom (one time operation), this protocol does not require any specialized skillset and can be completed within 4–5 h.

Key points

- Protocol for an in vitro sensor to measure cell traction force, matrix remodeling and biomechanical assays in self-assembled 3D tissues, including detailed steps for manufacturing the sensors, preparing the experimental setup, developing assays with different tissues and for imaging and analyzing the data.
- This approach enables quantification for cells in a 3D environment with extracellular matrices around them, which more closely resembles the in vivo setting than 2D approaches.

Key references

Emon, B. et al. *Sci. Adv.* **7**, eabf2629 (2021): https://doi.org/10.1126/sciadv.abf2629

Joy, M. S. H. et al. *Proc. Natl Acad. Sci.* **120**, e2311995120 (2023): https://doi.org/10.1073/pnas.2311995120

Emon, B. et al. *Acta Biomater.* **173**, 93–108 (2024): https://doi.org/10.1016/j.actbio.2023.11.015

[1]Department of Mechanical Science and Engineering, University of Illinois at Urbana–Champaign, Urbana, IL, USA. [2]CZ Biohub Chicago, LLC, Chicago, IL, USA. e-mail: saif@illinois.edu

Introduction

The cell–matrix interaction is the most important component in mechanotransduction, and has vital roles in various physiological and pathological processes, such as wound healing[1,2], fibrosis[3], angiogenesis[4], migration[5,6] and cancer[7–12]. Communications between cells and surrounding extracellular matrices (ECMs) is primarily mediated through cellular forces that provide the link between physical cues and chemical signaling. This creates a dynamic reciprocity[13–17] between cells and the surrounding microenvironment (ME). One of the most critical aspects of cell–ECM interactions is the feed-forward relationship between cell contractility and matrix remodeling. The dynamics of cell force and ECM remodeling have been implicated in numerous biological processes and disease progression[7,18–33]. Therefore, measurement of traction force in association with matrix remodeling is extremely important. As a result, methods to quantify cell traction on two-dimensional (2D) substrates have been developed and advanced over the past decades. However, cells in vivo are in a three-dimensional (3D) environment with ECM around them. There is a gap in the literature for methods to directly quantify cell traction and cell-induced matrix remodeling in 3D. We have developed a sensor[34] for direct measurement of single-cell forces and determination of matrix remodeling in 3D ECM as a function of time. Here, we present the detailed methodology for manufacturing the sensors, preparing the experimental setup, forming different types of tissues and imaging and analyzing the data.

Development of the protocol

The ultrasensitive sensor we describe here is inspired by previous devices that measure force from a large number of cells in 3D matrices[35,36]. We designed the sensor so that a tissue construct, consisting of various cells and matrices, can self-assemble and self-integrate with the sensor. The tissue can have single or multiple cells embedded in a 3D ECM. For example, we have demonstrated our sensor with in vitro tissue models of colorectal and lung carcinoma with fibroblasts and cancer cells[34]. In a recent study, we also constructed hippocampal neuron networks on the sensor to measure axonal tension[26].

The sensor is prepared by casting polydimethylsiloxane (PDMS) in silicon molds micro-fabricated with standard photolithographic process. With a resolution of ~1 nN, the sensor is capable of directly quantifying single cell forces in collagen (ECM), using force equilibrium law that allows circumventing complicated constitutive relations[24,34]. In addition, we further demonstrate that the sensor can be used as an actuator to measure change in ECM stiffness due to remodeling as a function of time, as well as to apply prescribed stretch or compression on the cell–ECM matrix to explore cell response to mechanical deformation in 3D. Hence, the sensor offers a platform with a range of applications for biophysical investigations of cells and tissues.

Concept and validation

The sensor consists of three components: a soft spring (spring constant, K_s), a stiff spring (K_r) and two grips connected to the springs as shown in Fig. 1. The soft spring is the force sensing element, while the stiff spring stabilizes the specimen that is self-assembled between the grips. The specimen is formed by dispensing a precursor solution (e.g., Matrigel, cell–collagen mixture, etc.) on the grips and allowing it to polymerize and self-assemble in situ (Fig. 1a). After formation of the specimen, the cell(s) activate within the matrix and generate contractile force (F), which deforms the soft spring. If the initial and contracted lengths of the sample, i.e., the gap between the grips, are denoted as L_0 and L_c, respectively, then the deformation of the sensing spring is given by $\delta_c = L_0 - L_c$, since the stiff spring's deformation is negligible ($F/K_r \approx 0$) (Fig. 1a). The δ_c is measured from optical images and the force can be determined as $F = K_s \times \delta_c$. The sensor also allows manipulation of the specimen, such as stretching and compressing, which enables measurement of mechanical properties, e.g., stiffness. Figure 1b shows the technique for measuring tissue stiffness. Here, initial length of the tissue specimen before actuation is denoted as L'_0. For measuring compressive stiffness, the tissue is compressed so that the specimen length is L'_c and the sensing spring deformation is δ'_c. Hence, the tissue

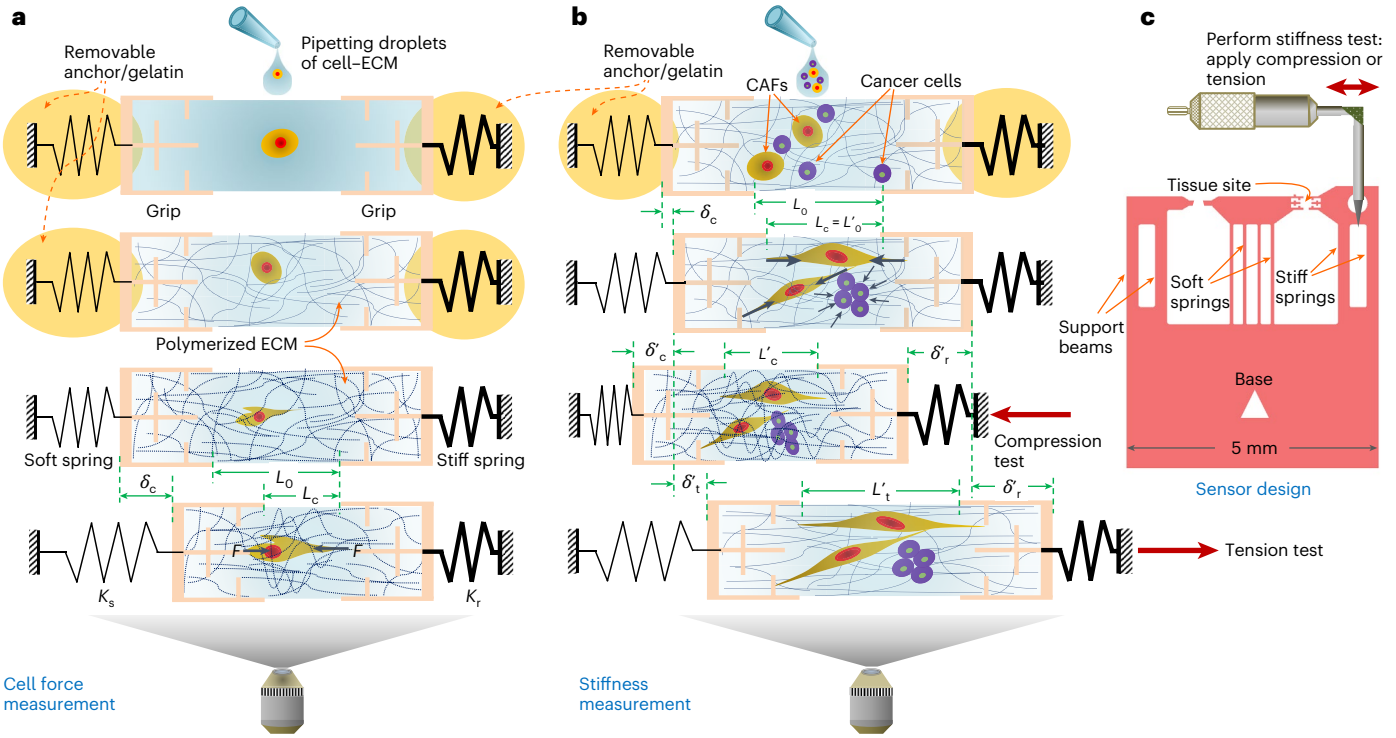

Fig. 1 | A schematic illustration of the concept, design and functional mechanics of the sensor. a, A simplified representation of self-assembly of a specimen and measurement of cell force in 3D matrices. First, the springs of the sensor are immobilized using gelatin. A tissue is formed by applying a cell–ECM mixture and allowing the ECM to polymerize between grips. With time, the cell(s) activate and engage with ECM fibers and generate contractile force that transfers to the springs and deform the soft spring (spring constant = K_s). Using a microscope, movement of the grips are tracked, deformation of the springs is measured and cellular activities are observed. The cell force is quantified as the product of spring constant and deformation ($K_s \times \delta_c$). **b**, The technique for measurement of stiffness of the tissue on the sensor. Stiffness of the tissue can be measured by applying axial compression and/or tension to the tissue. Using a linear stage, the stiff beam is pushed or pulled, while continuously monitoring spring deformation and grip movement to measure force and strain. **c**, A simple design of the sensor shows different components. The thin and wide beams represent soft and stiff springs respectively. The circular hole provides access to the needle connected to micrometers for manipulating the tissue for stiffness measurement.

deformation is $\Delta L'_c = |L'_c - L'_0|$ and the axial compression force on the tissue is $F'_c = K_s \times \delta'_c$. The relationship between F'_c and the $\Delta L'_c$ offers insight on the biophysical property of the tissue sample. For linear force-displacement curves, tissue stiffness can be measured as $K_c = \frac{F'_c}{(\Delta L'_c)}$. For non-linear relations, fitting the force-deformation curve to a suitable non-linear model, the tissue stiffness can be determined as $K_c = dF'_c/d(\Delta L'_c)$ at $\Delta L'_c$. For measurement of tensile stiffness, the specimen can be stretched as shown in Fig. 1b, and the stiffness is determined as $K_t = \frac{F'_t}{(\Delta L'_t)}$ or $dF'_t/d(\Delta L'_t)$ at $\Delta L'_t = L'_t - L'_0$, where $F'_t = K_s \times \delta'_t$ is the axial tension and deformation of the sample is $\Delta L'_t$. Figure 1c illustrates a design of the sensor and a technique of mechanical testing.

Next, we discuss the mechanism of force transmission from the matrix to the sensor and how to interpret the force readout. In theory, force applied within the matrix must be balanced. We argue that the majority of the applied force is balanced by the sensor spring. In a simplified system, the collagen matrix between the grips of our sensor can be considered as a spring in series with the sensor spring (Fig. 2a). Collagen spring, however, has a special property: it can take tensile force, but buckles under compression. This is true for any fibrous ECM. Fibers can take tensile force but buckle under small compressive force. Hence, any force on collagen, far from the sensor, is transferred almost entirely to the sensor's spring (Fig. 2a). A small fraction of the force is used to buckle collagen fibers. This fraction is not transferred to the sensor spring. Note that deformation of collagen due to any force can be different from that of the sensor spring due to the difference between their stiffness.

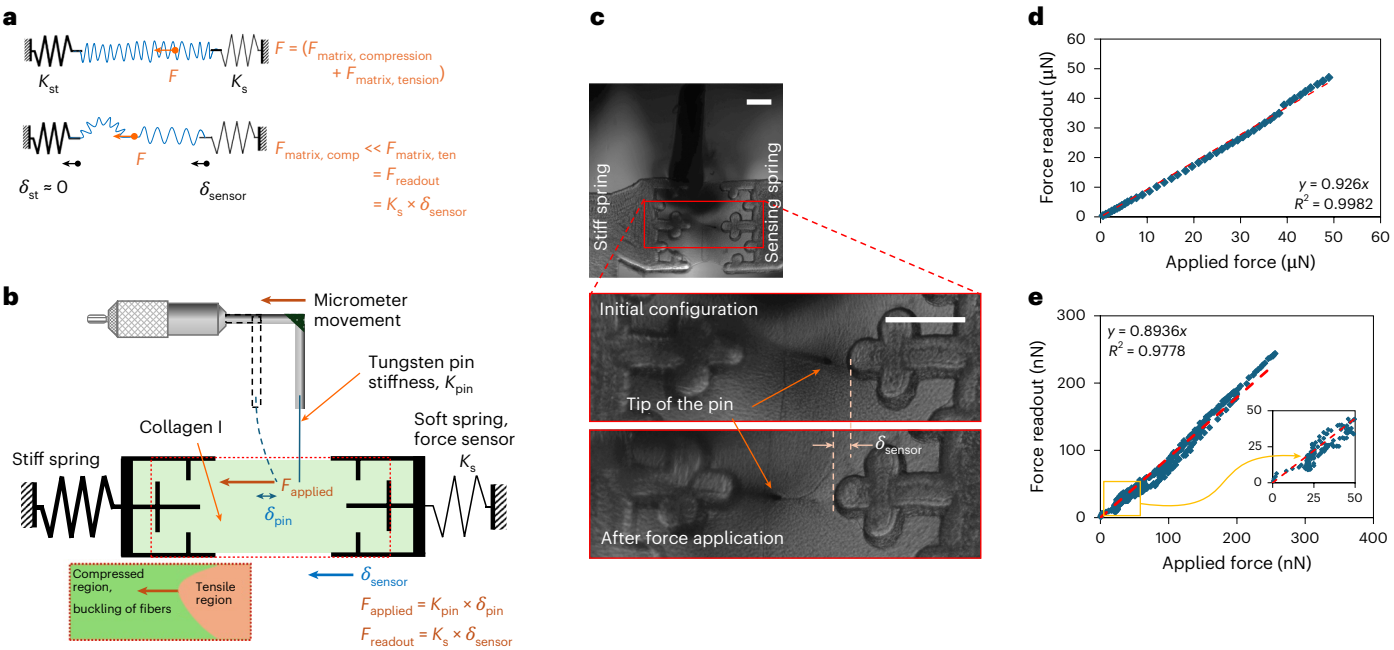

Fig. 2 | Transfer of a point force applied on the ECM to the sensor (force calibration). a, A schematic showing the mechanism of force transfer from the force point to the sensor through the ECM bridge. The ECM bridge serves as a spring that is in series with the sensor spring. Any force applied on the ECM, far from the sensor, must be transferred to the sensor spring for force balance. Collagen buckles under small compressive force. Hence, the soft sensor records the tensile component of the force, i.e., most of the applied force. **b**, The experimental setup to test force transfer from a point on ECM to the sensor springs. **c**, A tungsten cantilever pin (30 μm diameter, K_{pin} = 0.43 μN/μm) is attached to a micrometer that inserts the tip of the pin into the collagen specimen and moves the pin to apply tensile force on the ECM far from the sensor. The tensile region of the ECM transfers most of the applied force to the sensor, as collagen fibers in the compressed region provide very little resistance due to buckling. δ_{pin} and δ_{sensor} are measured from images and micrometer readings. $F_{applied} = K_{pin} \times \delta_{pin}$ and $F_{readout} = K_s \times \delta_{sensor}$. The calibrator pin is moved to the left, as the grip connected to the force sensing spring (on the right) moves by δ_{sensor} (Supplementary Video 1). **d**, The sensor detects applied force with high precision and the relationship between applied force and the sensor readout is linear. **e**, To calibrate force in the range of single cell contractility, a tungsten calibrator pin with K_{pin} = 3.9 nN/μm (20 μm diameter, 13.4 mm length) is used. Again, a similar relationship between applied force and the readout is observed. Scale bars, 500 μm.

We validated this argument by simply applying a known force at a point of the collagen bridge and by comparing the known applied forces with force readout by the sensor. We used a fine tungsten pin (30 μm in diameter, 4.8 mm in length) with known spring constants (0.43 μN/μm) to apply the forces. The base of the pin was held by a micrometer stage. To apply single point force, we brought the tip of the pin in contact with collagen bridge formed between the sensor grips (Fig. 2b), submerged in PBS at 37 °C. The base of the pin was then moved by the micrometer. The pin bent and applied a force on the collagen. The applied pin force was calculated from the bending of the pin and its spring constant. The pin force is transferred to the sensor grip through the collagen matrix. The sensor spring deformed as a result (Fig. 2c and Supplementary Video 1). The sensor force was calculated from its spring constant and its own deformation. We compared the force applied by the pin with that recorded by the sensor and the match is close to 93% (Fig. 2d). Seven percent of the applied force is 'lost' in compressing the collagen. Therefore, the force readout by the sensor is a conservative measurement, which is slightly smaller than cell generated force.

Overview of the procedure

Before starting the procedure, it is necessary to first design the sensor and fabricate the mask. The sensors can be designed as single units or as an array of connected sensors for high throughput applications. The array of sensors on the mask can be drafted such that a 4 inch wafer can accommodate ~100 sensor units. The mask making can be outsourced to fabrication facilities that can create masks from design (i.e., computer-aided design (CAD) files, a sample

is available as Supplementary Data 1). Further considerations on sensor design are discussed in the 'Experimental design' section. The next stage is to microfabricate the silicon molds in a cleanroom, as illustrated in Fig. 3a (Steps 1–12). A standard photolithography process can be used to spin-coat photoresist, expose to UV and develop a wafer, which is then etched to a desired depth by deep reactive-ion etching (DRIE) technique (Steps 1–9). The final stage in preparation of the molds is coating the etched wafer with polytetrafluoroethylene (PTFE) that facilitates removal of the sensors from these templates (Steps 10–12). Such silicon molds can be used many times, if carefully used and kept clean. Finally, the sensors can be prepared by pouring liquid PDMS in the casts, polymerizing and removing from the molds, as shown in Fig. 3a (Steps 13–21). The sensors are calibrated after they are removed from the mold, preferably just before setting up the experiment (before Step 22).

Figure 3b presents a step-by-step procedure for preparation of the experimental setup (Steps 22–40). First, a thin gelatin layer is prepared to prevent the sensor from touching and sticking to the bottom glass (Steps 22–24). Next, the sensor is positioned on site and additional gelatin is added to immobilize the springs (Steps 25–27). After that, the tissue precursor solution is dispensed and allowed to polymerize into the final specimen (Steps 28–33). Finally, culture medium is added to the dish when gelatin dissolves and gets washed out in ~30 min at 37.5 °C (Steps 34–35). The sensor is thus released and activated for force measurement. We provide steps for constructing different tissue configurations: type I tissue with a single cell, a few cells or a coculture of multiple cells (Fig. 4); type II tissue with similar cells in the grips only,

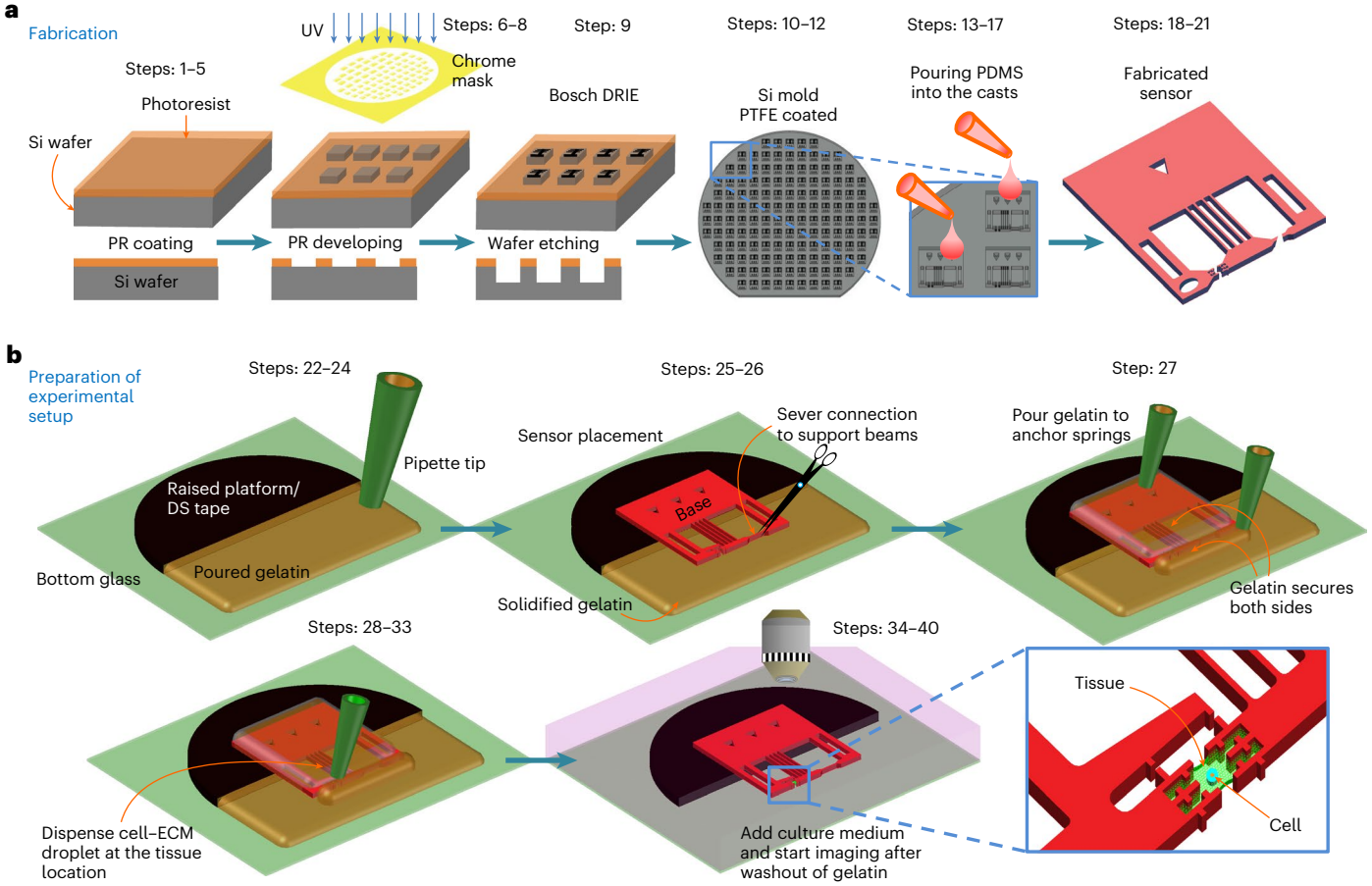

Fig. 3 | Fabrication of the sensors and preparation of experimental setup. **a**, Photolithography and microfabrication process for preparation of the silicon molds (Steps 1–12). The PDMS sensors are cast from the molds by pouring liquid PDMS and curing at 60 °C overnight (Steps 13–21). **b**, The sequence of operation for preparation of the experimental setup (Steps 22–40). This methodology helps the sensors overcome surface energy related challenges. Further illustrations for Steps 27–33 are shown in Figs. 3–5.

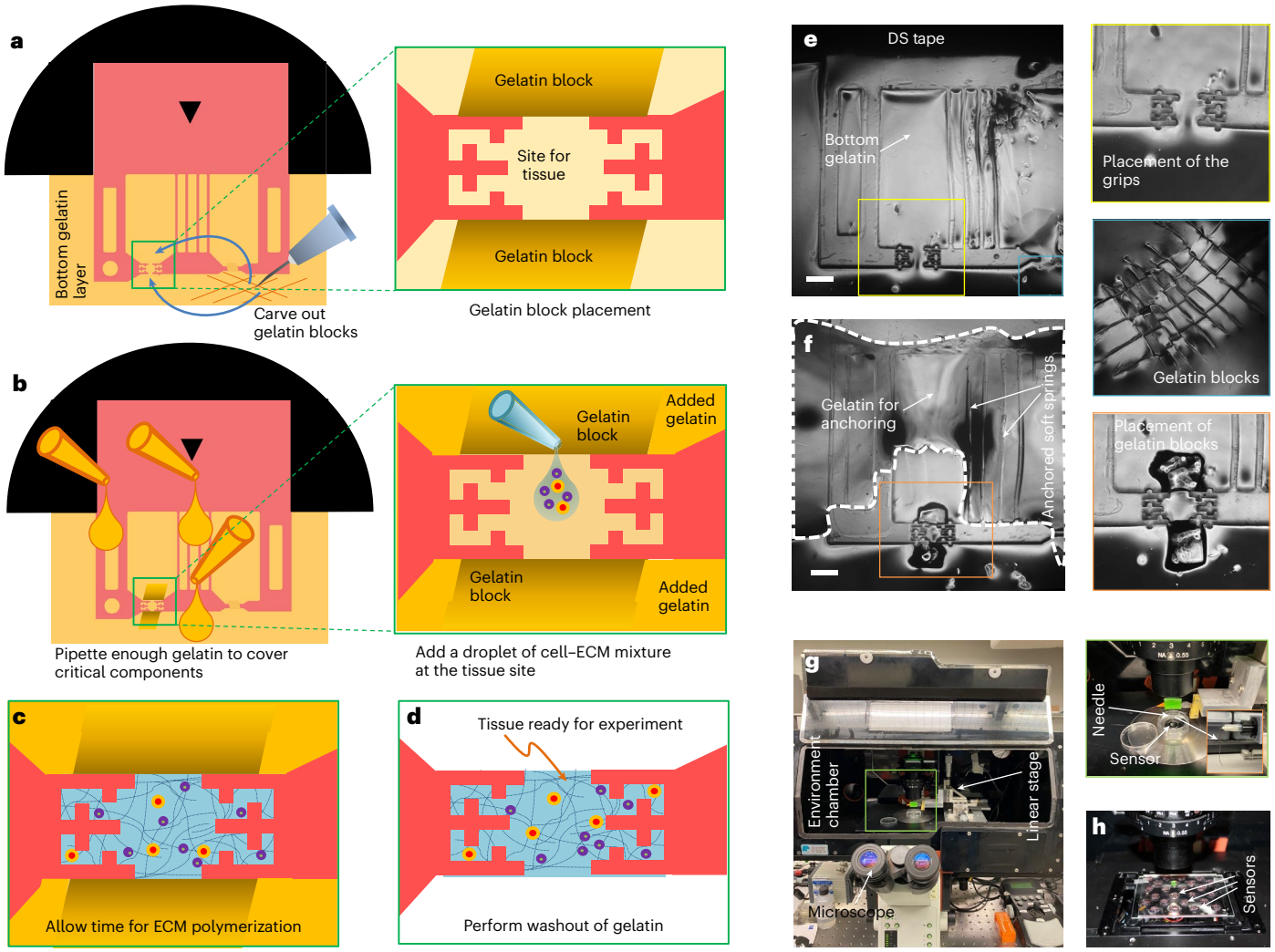

Fig. 4 | Detailed illustrations for tissue construction with cells in all parts of the tissue. a, Placement of gelatin barriers to secure tissue formation site (Step 27A(i)). **b**, The addition of gelatin to anchor the springs (Step 27A(ii)) and pipetting cell–ECM mixture (Step 33A(i)). **c**, The application of negative pressure in a vacuum desiccator and polymerization of ECM for self-assembly of the tissue construct (Step 33A(ii–iv). **d**, Release of the springs (Steps 34–35). **e**–**h**, Images of the experimental setup showing placing the sensor on the bottom gelatin layer, the prongs of the grips should be detached from each other and the distance between the grips should be similar to the design tissue length (**e**); the gelatin blocks placed on the sensor except the grip region (**f**) (the dashed white line indicates the boundary of the additional gelatin used as anchors for springs); the setup for stiffness measurement with a motorized stage (**g**) and the array of sensors, each in separate wells for high-throughput applications, e.g., drug screening (**h**). Scale bars, 200 µm.

with the central region constructed of cell-free ECM (Fig. 5); and type III tissue with two types of cells in two grips, keeping the central portion free of cells (Fig. 6).

We then describe the procedure for force data acquisition, tissue stiffness testing and calibration of the sensor's spring constant. For longitudinal force measurement, data are collected with brightfield or phase contrast imaging of the tissue (Steps 36–40). Next, to measure tissue stiffness, axial compression or tension is applied by pushing or pulling the tissue, while imaging the sample simultaneously (Steps 41–47). The steps can also be used to assess matrix remodeling by cells, by measuring the initial stiffness right after gelatin is washed out at Step 35, and then measuring stiffness every 24 h to determine the extent of mechanical remodeling of the matrix by the cells. Data collected in Steps 36–47 are then analyzed with ImageJ software to determine cell force and tissue stiffness (Steps 48–54). Lastly, to maintain accuracy of measurement, a method is described to calibrate the sensor's spring constant (Steps 55–59).

Comparison with other methods

It is well established that cell traction force is at the center of most biophysical processes and, consequently, extensive research went into investigation of cellular forces. However, most of the methods developed for measuring cell generated forces are on 2D substrates, e.g., traction force microscopy (TFM)[37–39], Förster resonance energy transfer[40] and micro-pillar arrays[41]. These techniques are widely used at present, but the majority of them are limited to 2D culture. For example, a protocol by Zhang et al.[39] describes TFM for cells on 2D hydrogels. While 2D cell culture is convenient and has provided important insights into biophysical processes, cells in 3D matrices may respond very differently. Hence, quantification of cell force in 3D matrices is of utmost importance. Despite the great necessity, currently available techniques can only measure force if the number of cells is large (~1,000 cells)[35,36]. In addition, most natural fibrous matrices (e.g., collagen, Matrigel and fibrin) in 3D are heterogeneous at cellular scales and hence do not exhibit simple constitutive relations. Moreover, cells continuously remodel the scaffolds by ECM deposition, cross-linking and force-induced plastic strains. Hence, a constant elastic modulus cannot be used to determine cell forces. The protocol presented describes a novel approach to determine cell-generated forces in 3D by direct measurement from force balance, bypassing such spatio-temporal variations of the mechanical properties of the ECM. Compared with other procedures, this is the most notable advantage of our protocol.

There are a few computational methods, such as kinematics-based mean deformation metrics[42] and the finite element approach such as 3D TFM[43–45] that can estimate cell generated deformation and thus approximate forces in 3D. However, limitations of these methods include the assumptions of constitutive equations (stress–strain relations), computationally expensive analysis and/or use of fluorescent lights with damaging intensities[46]. For example, Piotrowski et al.[45] assumed collagen to be linear elastic with constant modulus of elasticity, which serves only as a first approximation. Again, Afthinos et al.[44] used polyacrylamide gels that are linear elastic to avoid this assumption. However, polyacrylamide gels do not present physiologically relevant fibrous scaffolds for the cells to remodel. Also, fluorescent light used to track beads may have affected cell traction forces[46]. Our protocol is free from these drawbacks. In fact, by analyzing

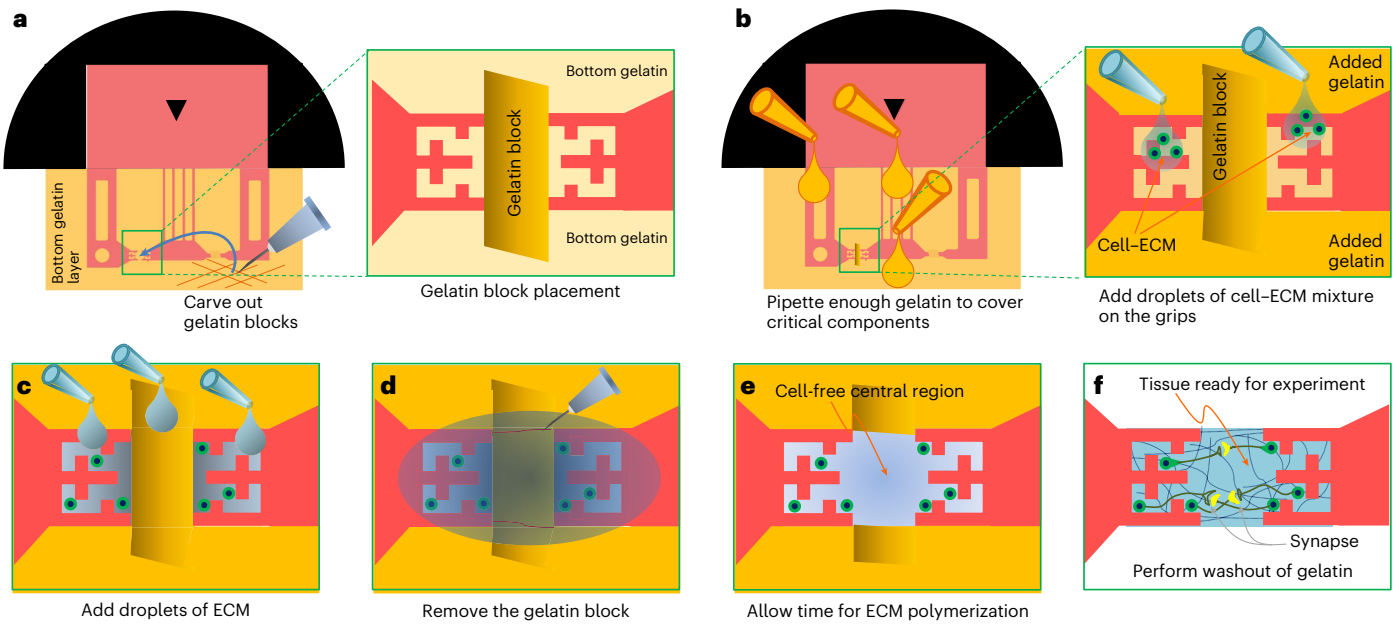

Fig. 5 | Detailed illustration for tissue construction with cells inside the grips and the central region is cell free. a, Placement of gelatin barriers to block central region of the tissue site (Step 27B(i)). **b**, The addition of gelatin to anchor the springs (Step 27B(ii)), pipetting cell–ECM mixture and applying negative pressure (Step 33B(i–ii)). **c**, Removal of excess cell–ECM mixture (Step 33B(iii)) and addition of a droplet of cell-free ECM (Step33B(iv)). **d**, Removing the central gelatin block to allow ECM to fill in the space (Step 33B(v)). **e**, Polymerization of ECM for self-assembly of the tissue construct (Step 33B(vi–vii)). **f**, Release of the springs (Steps 34–35).

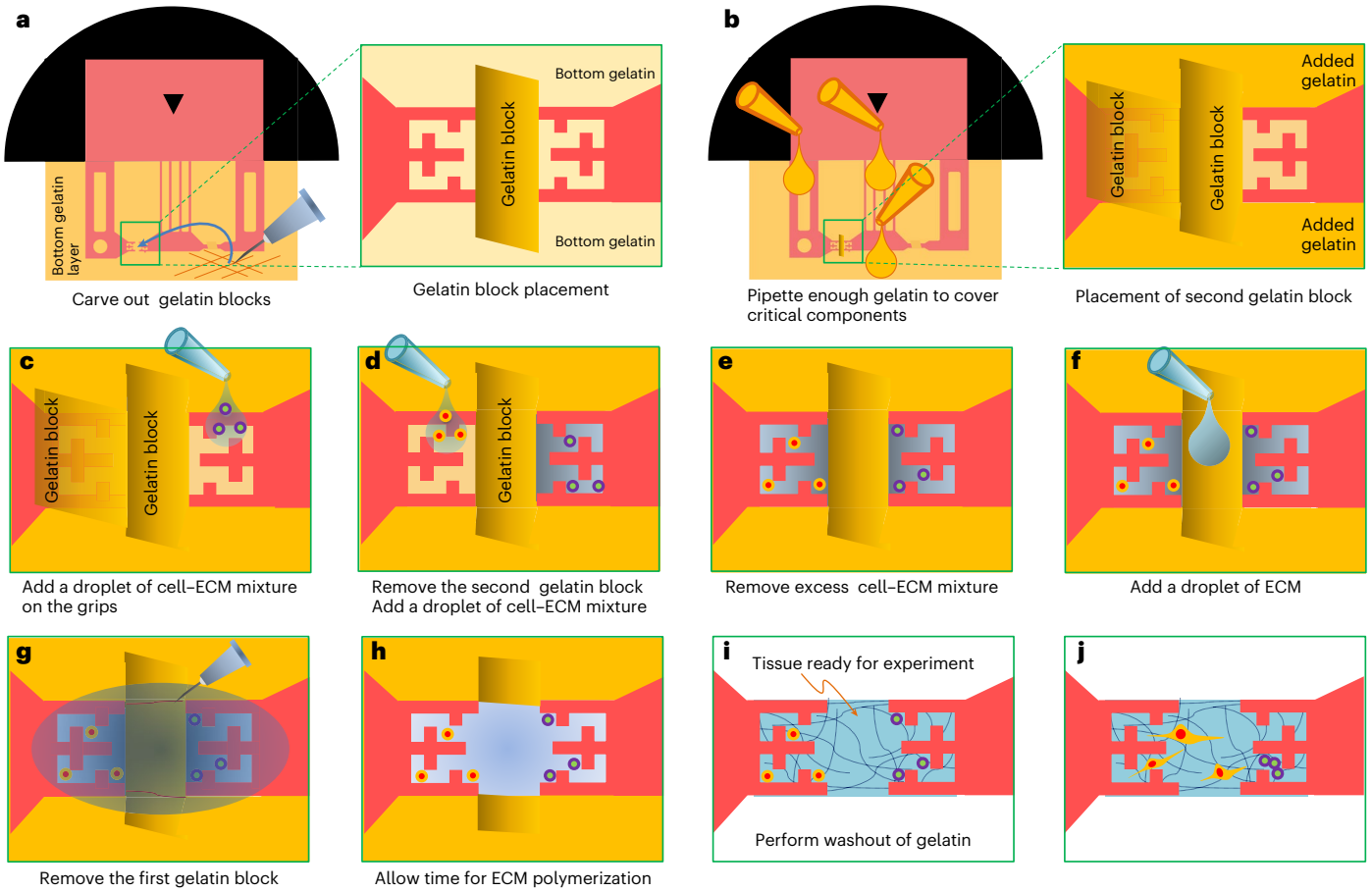

Fig. 6 | Detailed illustration for tissue construction with two types of cells in two grips and the central region cell free. a, Placement of gelatin barriers to block central region of the tissue site (Step 27C(i)). **b**, Addition of gelatin to anchor the springs (Step 27C(ii)) and placement of another gelatin block on one of the grips (Step 27C(iii)). **c**, Pipetting cell–ECM mixture and applying negative pressure (Step 33C(i–ii)). **d**, Removal of excess cell–ECM mixture (Step 33C(iii)), removal of the gelatin block on the grip (Step 33C(iv)) and addition of a droplet of second cell–ECM mixture (Step 33C(v)). **e**, Application of negative pressure (Step 33C(vi)) and removal of excess cell–ECM mixture (Step 33C(vii)). **f**, Addition of a droplet of cell-free ECM (Step 33C(viii)). **g**, Removing the central gelatin block to allow ECM to fill in the space (Step 33C(ix)). **h**, Polymerization of ECM for self-assembly of the tissue construct (Step 33C(x–xi)). **i**, Release of the springs (Steps 34–35). **j**, Cells migrate into the central region providing corresponding force and stiffness changes.

phase-contrast images using simple ImageJ plugins, it is possible to calculate the forces in real time. Moreover, the lack of fluorescent lights enables monitoring of force for a long duration.

In addition to cell forces, the sensor is capable of 'direct' measurement of stiffness of the specimen or tissue at different timepoints. This unique ability helps track the dynamics of ECM remodeling and traction force simultaneously. While there are methods that can provide 'indirect' quantification of remodeling[47], there are no other techniques currently available to directly assess cell force and matrix remodeling dynamics in the same tissue sample, which enables us to correlate force and stiffness. This is an advantage over other methods that cannot read both force and stiffness from the same specimen. Also, our previously developed silicon-based sensor[35] can measure stiffness of larger tissues; however, dissolved silicon in the culture media may have toxic effect on the cells[48].

Besides stiffness, cells transduce other mechanical stimuli such as stretch and/or contraction into electrical and/or biochemical signals for functions relevant in many organs such as lung alveoli, bladder or the heart[49–54]. To study the role of cellular stretching in signaling pathways, devices have been developed to apply mechanical stretch to cells and determine their stress–strain relationship[55–58]. However, most of these devices rely on elastomeric membranes for applying stretch to 2D substrate-adhered cells. Even if the cells are embedded in 3D ECM on

top of these membranes, they sense the rigidity of the membranes and thus the setup falls short in representing the in vivo environment. The sensor presented herein eliminates this limitation by creating a self-organized tissue that does not require support from such stiff membranes. Hence, cells in the specimen are truly in 3D scaffold that better mimics in vivo ME.

Limitations

The sensor has a few limitations. First, the sensor can only measure the total cell force, and local traction stresses within the matrix cannot be determined. However, addition of fiducial beads in the matrix may facilitate reconstruction of 3D deformation field and compute an approximation of local stresses. Also, the sensor is not sensitive to molecular-level forces experienced by transmembrane proteins such as integrins. Recently developed molecular probes such as DNA-based sensors[59] or quantum probes[60] can be utilized to measure subnanoNewton tensions generated at focal adhesions sites. Currently, these methods are verified on 2D substrates. However, if these technologies are modified for 3D, they can complement the sensor by extending the range of force detection. Another limitation is brightfield or phase-contrast imaging. While these imaging methods are sufficient for force measurement and 2D projected visualization, tomographic imaging, e.g., confocal, two-photon microscopy, is necessary for accurate 3D spatial correlations.

Applications

The greatest strength of the sensor is adaptability and versatility. As a result, the sensor and the self-assembled specimen can be modified for multifunctionality without major investments. Table 1 presents several prospective applications of the sensor and the protocol. For example, by simply adding 1 µm polystyrene (PS) beads in the scaffold and confocal imaging, we can potentially detect local deformations in addition to the total force by the cells. The local deformation field can provide vital information pertinent to specific cellular activities such as polarization and migration. Also, by precise placement of cancer and stromal cells at a distance, it is possible to investigate the role of both biochemical and biophysical cross-talk within tumor ME. Furthermore, it is conceivable that the sensor platform can be scaled up for translational application such as personalized drug screening with patient-derived primary cells. Commercially mechanizing a few steps of the process, it is possible to develop a high-throughput system for clinical assays that can leverage biophysical outputs (i.e., traction force, ECM remodeling, effects of drugs) from the sensors.

Table 1 | Potential applications of the protocol

Graphical representation	Experiments	Potential applications	Relevant literature to consult
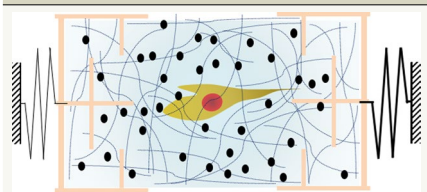	Addition of fiducial beads in the ECM and cells	Investigation of cell–matrix interaction in various biological processes	25,42,79
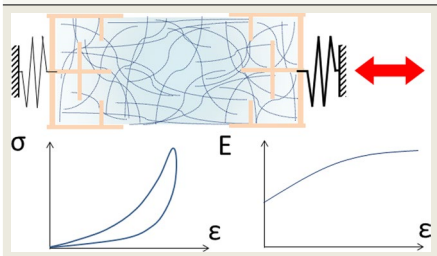	Axial loading test on self-assembled specimens	Mechanical characterization of natural and synthetic biopolymers and active matters	24,80–82

Table 1 (continued) | Potential applications of the protocol

Graphical representation	Experiments	Potential applications	Relevant literature to consult
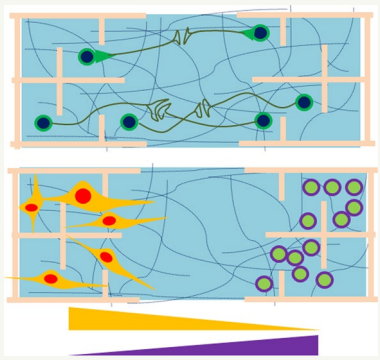	Biomechanical interaction between cells at a certain distance	Neuronal synapse connections and axonal tension studies; investigate cancer cell–stromal cell feedback dynamics	7,11,22,26,83,84
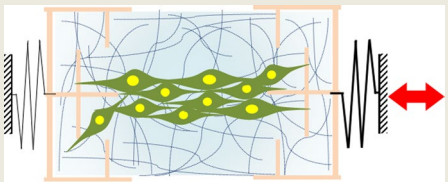	Applying strains to cells	Investigating response to strains from cells, e.g., cardiomyocytes, muscle cells and fibroblasts, that undergo strains in vivo	49–54
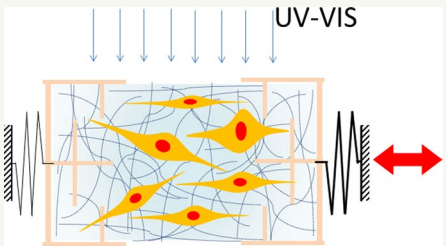	Radiation therapy on the ex vivo tissues	Corneal collagen cross-linking for keratoconus therapy; studying radiotherapy for cancer treatment	85–89
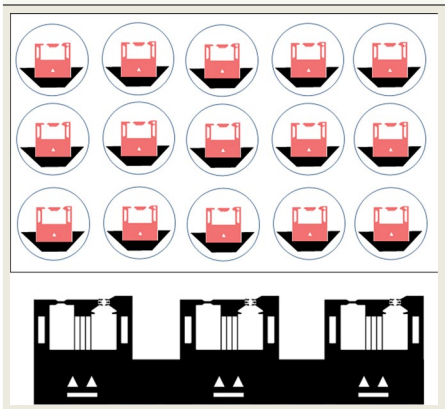	High-throughput setup for drug screening	Personalized cancer and fibrosis models for phenotypic screening or drug efficacy tests with primary cells	90–94
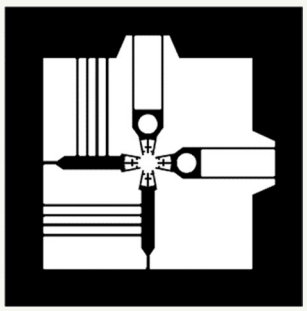	Biaxial sensor with shear deformation measurement capacity	Measurement of cell forces resolved in two axes, bi-axial material testing	

In addition to measuring cell generated forces and remodeling of ECM, the sensor provides a unique platform for material testing and manipulation at microscale. For example, the sensor enabled utilization of non-linear elasticity (i.e., strain-stiffening for collagen) to control of matrix stiffness on demand[24]. Potential applications for future can be investigation of emergent behavior in active matter systems (e.g., F-actin–myosin II network). The sensor leverages self-organization of such material systems and formation of the sample. It is virtually impossible to construct samples of such small scales and perform tensile or compressive tests otherwise. Furthermore, by applying a prescribed amount of strain, we can possibly manipulate microstructures in the sample, e.g., fiber orientation, pore sizes and anisotropy, and thus study the effects of microstructural changes on their dynamics of their macroscopic properties. We propose a few prospective applications below (Table 1). They serve as a guide to customize and utilize the sensor for transformative applications.

Experimental design

In designing new experiments with the sensor, several key factors should be considered to ensure accurate and reproducible results. First, the sensor's spring constant should be determined considering the type and number of cells, and should be calibrated if the PDMS curing method is altered or a different silicone material is used. Second, force transmission within the ECM should be calibrated, especially when the matrix is structurally different from fibrous scaffolds such as collagen, Matrigel or fibrin. Third, acellular ECM controls should be included to account for any matrix-intrinsic forces and/or extraneous noise. Also, a minimum of three replicates per condition is recommended to ensure statistical significance. Finally, imaging frequency for force dynamics is determined based on the anticipated rate of contractility, while the time interval between stiffness measurement is decided on the matrix remodeling capacity of the cells. For example, fibroblasts have high rate of contractility and matrix remodeling capacity; hence, we image every 5 min for force dynamics and test stiffness every 24 h. By contrast, neurons have slow contractility, and thus we image every hour and measure stiffness every 3 days. Also, stiffness can be dependent on the strain rate, especially for viscoelastic materials. Therefore, displacement rate should be consistent between experiments, and we found 10 μm/s to be reasonable for our experiments. By addressing these key aspects, researchers can adapt the protocol to their specific experimental needs and ensure reliable measurements of cell forces and matrix remodeling in 3D matrices.

As an example, the sensor's design is shown in Fig. 1c. The soft spring is comprised of a set of narrow beams and the stiff spring is made up of thick beam(s). For a uniaxial sensor, the ends of the beams are connected to a frame that restricts rotation and only allows translation along the x axis. The other ends of the beams are fixed to the base of the sensor and have zero degrees of freedom. In addition, the stiff beam (spring) has a hole that allows a needle to latch onto it (Fig. 1c). To measure tissue stiffness, the needle is connected to a linear stage equipped with three micrometers (x-y-z directions). The micrometers are used to precisely position the needle into the hole and move the left (for compression) or right (for tension), as illustrated in Fig. 1c. This is a simple design of the sensor; however, complex sensors can be designed for more sophisticated applications (not demonstrated here). For the case of using beams as springs, readers should be careful when determining spring constants (i.e., stiffness). Loading and boundary conditions govern deflection of beams and hence, stiffness. Sensor beams shown in Fig. 1 deform under shear and flexure, so that with the stiffness for n beams can be calculated as $K_s = 12\,nEI/L^3$, where E, I and L are modulus of elasticity of PDMS, moment of inertia about bending axis ($I = hb^3/12$, with b and h being the width and depth of the beams) and length of the beams, respectively (details in refs. 61–65).

The design specifications for the sensor mainly depend on the anticipated force generated by the cell(s). For example, a tissue with neurons produces ~10–50 nN (ref. 26) or a tissue with cancer-associated fibroblasts (CAFs) may produce ~100–500 nN (ref. 34). To reliably read this force, the sensor's soft spring constant (K_s) should be so chosen that deformation δ_c can be precisely detected from images (generally, $\delta_c > 1\,\mu m$ is sufficient for typical brightfield microscope cameras). The dimensions of the beams (width and length provide the most leverage) are determined based on the target K_s. For instance, to measure neuronal force,

the soft spring can be designed as four parallel beams with dimensions of 30 µm in width, 200 µm in depth and 2,000 µm in length. The resulting spring has K_s = 4.6 nN/µm (with E for PDMS being 1.7 MPa) and should have $\delta_c > 2$ µm with anticipated peak force, F >10 nN. To measure higher forces (e.g., by the CAFs), we increased the spring stiffness by changing the beam width to 50 µm (K_s = 21.3 nN/µm). A template (CAD file) is provided to aid design (Supplementary Data 1). It is important to calibrate the sensor's spring constant to ensure reliability of the data. Calibration can be performed before the experimental setup (i.e., before starting Step 22) or after the force and stiffness data collection (i.e., after Step 46) by removing the sample with collagenase (e.g., 100 U/ml collagenase type II, 12 h at 37 °C).

These sensors are extremely adaptive and can be designed for diverse biophysical assays. By altering the dimensions of the beams (springs), high sensitivity can be achieved for measurement of single-cell forces in 3D matrices. With increasing force resolution, the beams become very soft and susceptible to collapse (i.e., buckling, twisting or sticking to each other) due to meniscus forces (surface tension) that they are subjected to at different stages of operation. The protocol described here helps tackle this challenge. In essence, the soft elements of the sensor are immobilized (as illustrated in Fig. 1) by a gelatin sacrificial layer that can be removed after the completed test assembly is immersed in culture media. This unique approach is one of the key contributions of this protocol. In addition to the sensor's adaptability, the protocol describes multiple types of tissues for different applications. For example, type I tissues (Fig. 4) are suitable to assess contractility and matrix remodeling in muscle models, fibrosis models or tumor models where cancer and stromal cells are monocultured or cocultured. Type II tissues (Fig. 5) are targeted for studies on cells such as neurons and astrocytes that grow neurites and generate tension for function. Type III tissues (Fig. 6) are equipped for biomechanical investigation of cross-talk between two different types of cells such as muscle cells and motor neurons or cancer and stromal cells. In addition, the sensors can be used to longitudinally measure mechanical properties of soft and active materials (with or without cells) that remodel for intrinsic or extrinsic mechanisms. Moreover, these sensors can be assembled in arrays with separate wells for a high-throughput applications such as drug screening.

Materials

Biological materials

▲ **CAUTION** Human cancer related cells should be handled in a BSL-2 laboratory with approval of relevant institutional review board (IRB).

- FET human colorectal cancer cell line (a gift from Barbara Jung's lab at UIC medicine) (https://scicrunch.org/resolver/RRID:CVCL_A604)
  ▲ **CAUTION** Cell lines used in research should be regularly checked to ensure they are authentic and are not infected with mycoplasma.
- CAF05 human colorectal tumor CAFs (Neuromics, cat. no. CAF05)
  ▲ **CAUTION** Cell lines used in research should be regularly checked to ensure they are authentic and are not infected with mycoplasma.
- Primary CAFs (PrCAFs) (extracted[66] from patient-derived colorectal cancer tissue and sorted out[67] from cancer and other stromal cells)
  ▲ **CAUTION** Informed patient consent is required for the use of human tissue, and all studies must adhere to institutional and governmental ethical and technical guidelines on the use of human samples for biomedical research purposes. Our work was approved under IRB #14051 (2017) by the IRB at Carle Foundation Hospital.
- Primary mouse hippocampal neurons (harvested from day 18 embryonic (E18) mouse hippocampi using standard protocol[68]
  ▲ **CAUTION** Animal experiments should be performed according to the relevant institutional and national guidelines and regulations. Our work was approved under Protocol #22057 by the Institutional Animal Care and Use Committee at the University of Illinois.

Reagents

▲ **CAUTION** Always handle potentially harmful reagents in a fume hood while wearing appropriate protective equipment (e.g., wear gloves, protective eyewear and a laboratory coat).

- Vitroplus III, low serum, complete medium (Neuromics, cat. no. PC00B1)
- Fibroblast growth medium-2 bulletkit (Lonza, cat. no. CC-3132)
- Dulbecco's modified Eagle medium (DMEM) (Corning, cat. no. 10-013-CV)
- Hams F-12 medium (Corning, cat. no. 10-080-CV)
- Fetal bovine serum (FBS) (Gibco, cat. no. 26140079)
- Penicillin–streptomycin (Lonza BioWhittaker, cat. no. 17-602E)
- Oxaliplatin (Sigma-Aldrich, cat. no. O9512)
- Dulbecco's phosphate-buffered saline (DPBS) (Corning, cat. no. 20-031-CV)
- 2-Propanol (IPA) (Fisher Chemical, cat. no. 67-63-0)
- 500 µm silicon wafers (University wafers, cat. no. 3514)
- Sylgard 184 Silicone Elastomer kit (Dow Corning, cat. no. 4019862)
- Rat-tail collagen I (Corning, cat. no. 354236)
- 10× PBS (Lonza BioWhittaker, cat. no.17-517Q)
- 1.0 N Sodium hydroxide solution (Sigma-Aldrich, cat. no. S2770-100ML)
- Molecular biology grade water (Corning, cat. no. 46-000-CM)
- Gelatin (from bovine skin) (Sigma-Aldrich, cat. no. G9391)
- 16% (wt/vol) paraformaldehyde solution (Fisher Scientific, cat. no. 50-980-487)
- P.27 50× supplement (Invitrogen, cat. no. 17504-044)
- Neurobasal medium (Invitrogen, cat. no. 2I103-049)
  ▲ **CAUTION** Toxic and carcinogenic; can cause skin, eye, and respiratory irritation. Handle carefully.
- Triton X-100 (Sigma-Aldrich, cat. no. X100)
  ▲ **CAUTION** Harmful if inhaled or ingested; can cause skin and eye irritation. Handle carefully.
- Bovine serum albumin (BSA) (Sigma-Aldrich, cat. no. A1933)
- Normal goat serum (NGS) (abcam, cat. no. ab7481)
- Primary antibodies:
  - Anti-MAP2 (abcam, cat. no. ab5392; https://scicrunch.org/resolver/RRID:AB_2138153)
  - Anti-Homer (Invitrogen, cat. no. PA5-21487; https://scicrunch.org/resolver/RRID:AB_11155843)
  - Anti-Bassoon (abcam, cat. no. ab82958; https://scicrunch.org/resolver/RRID:AB_1860018)
- Secondary/conjugated antibodies:
  - Goat anti-chicken Alexa Fluor 488 (abcam, cat. no. ab150173; https://scicrunch.org/resolver/RRID:AB_2827653)
  - Goat anti-rabbit Alexa Fluor 568 (abcam, cat. no. ab175471; https://scicrunch.org/resolver/RRID:AB_2576207)
  - Goat anti-mouse Alexa Fluor 647 (abcam, cat. no. ab150115; https://scicrunch.org/resolver/RRID:AB_2687948)
- Phalloidin conjugated with Alexa Fluor 647 (Invitrogen, cat. no. A22287, https://scicrunch.org/resolver/RRID:AB_2620155)
- ProLong Diamond Antifade Mountant with DAPI (Invitrogen, cat. no. P36971)
- Positive photoresist: SPR 220-4.5 (Kayaku Advanced Materials, Inc., Megaposit SPR 220 i-Line series)
  ▲ **CAUTION** Flammable and may cause skin and respiratory irritation. Must be used in a chemical fume hood.
- Adhesion Promoter AP8000 (Dow Chemical, CAS no. 000107-98-2)
  ▲ **CAUTION** Flammable and may cause skin and respiratory irritation. Must be used in a chemical fume hood.
- AZ 400K developer (AZ Electronic Materials, CAS no. 1310-58-3)
  ▲ **CAUTION** Corrosive; can cause severe skin and eye burns. Must be used in a chemical fume hood.
- Acetone (Fisher Chemical, cat. no. 67-64-1)

- Microposit Remover 1165 (Fisher Scientific, cat. no. NC0305429)
  ▲ **CAUTION** Flammable and harmful; can cause skin and respiratory irritation. Must be used in a chemical fume hood.
- Riboflavin USP grade (MP Biomedicals, cat. no. MP210281305)
- Glutaraldehyde 70% (wt/vol) aqueous solution (Electron Microscopy Sciences, cat. no. 16360)
  ▲ **CAUTION** Toxic; can cause severe skin and eye irritation and respiratory issues. Must be used in a chemical fume hood.
- (3-Aminopropyl)trimethoxysilane (Sigma-Aldrich, cat. no. 281778)
  ▲ **CAUTION** Flammable and harmful; can cause skin and respiratory irritation. Must be used in a chemical fume hood.
- Ethanol 200 proof (Decon Laboratories, cat. no. 2701)

Equipment

- CAD file (the CAD used for our experiments is supplied as Supplementary Data 1)
- Chrome photomask (this must be available before starting this procedure. The mask can be made by commercial facilities, if supplied with the design drawing (CAD). For example, Arizona Micro Inc. fabricated our photomask)
- Biosafety cabinet (Baker, SterilGARD III Advance)
- Chemical fume hood (Fisher Hamilton)
- Nitrogen gun (VWR)
- Deep RIE machine (STS Pegasus ICP-DRIE)
- Pipettes (Gilson, model Pipetman)
- Stericup Quick Release-GP Sterile Vacuum Filtration System (Millipore Sigma, cat. no. S2GPU05RE)
- Waterproof 400 µm thick double coated tape (3M, cat. no. 1/2-5-5915)
- Tweezers (Aven, model 7-SA)
- Glass coverslips (Ted Pella, cat. no. 260156)
- Glass bottom petridishes (Cellvis, cat. no. D60-30-1-N)
- Plastic Petri dishes (Falcon, cat. no. 351008)
- Noyes Scissors sharp/sharp tips, straight (World Precision Instruments, cat. no. 500228)
- 27G × 1½ inch syringe needles (BD, cat. no. 301629)
- Pyrex crystalizing dish (Millipore Sigma, cat. no. CLS3140125)
- Spin coating machine (BidTec SP-100)
- PTFE deposition machine (Plasmatherm SLR 770)
- Oxygen plasma for cleaning (RIE-March Jupiter III)
- Hotplate (Thermo Scientific, Cimarec)
- Mask aligner (Electronic Vision, EVG-620, i-line)
- Cell culture incubator (New Brunswick, model Galaxy 170 S)
- Vacuum desiccator (Fisher Scientific, cat. no. 08-594-15C)
- Bubble level (Wyler, cat. no. 166-060-121-300)
- Oven (Cole-Parmer, Model 52120-02)
- Autoclave (Tuttnauer Brinkmann 3545E)
- Refrigerator
- Microscope with environment-control chamber (Olympus, IX81)
- Motorized stage (Prior Scientific, model H117P1I4/G)
- Motorized stage controller (Prior Scientific, model PS3J100)
- Vibration isolation table (Newport Corporation, RS4000)
- XYZ Linear Stage (MKS Newport, model MT-XYZ)

Software

- CAD software (AutoCAD 2019: https://www.autodesk.com/products/autocad)
- Imaging software (Metamorph Basic for Olympus IX81: https://www.moleculardevices.com/products/cellular-imaging-systems/acquisition-and-analysis-software/metamorph-microscopy#gref)

- Image analysis software:
  - ImageJ (https://imagej.nih.gov/ij/)
  - IMARIS (version 9.6.0, Bitplane AG, Zurich, Switzerland, https://imaris.oxinst.com/)

Reagent setup

Primary CAF culture medium

Prepare fibroblast growth medium by mixing 500 ml FBM Basal Medium, 0.50 ml insulin, 0.50 ml human fibroblast growth factor B (hFGF-B), 0.50 ml gentamicin sulfate–amphotericin (GA-1000) and 10 ml FBS (all provided with the fibroblast growth medium-2 bulletkit) and filtering through the Stericup filtration system. Once the components are mixed, the complete growth medium should be stored at 4 °C and used within 1 month.

FET cancer cell culture medium

Prepare FET culture medium by mixing 222.5 ml DMEM, 222.5 ml Hams F-12 medium, 50 ml FBS and 5 ml penicillin–streptomycin and filtering through the Stericup filtration system. The culture medium should be stored at 4 °C and used within 1 month of preparation.

Hippocampal neuron plating medium

Prepare Hippocampal neuron culture medium by mixing 50 ml FBS, 11.25 ml 20% (wt/vol) glucose in MEM, 5 ml sodium pyruvate (100 mM), 62.5 µl L-glutamine (200 mM), 5 ml 100× penicillin–streptomycin, 439 ml MEM Eagle's with Earle's balanced salt solution (BSS) without L-glutamine and filtering through the Stericup filtration system. Store the medium at 4 °C for up to 1 month and warm up to 37 °C before use.

Hippocampal neuron maintenance medium

Prepare Hippocampal neuron culture medium by mixing 10 ml P.27 50× supplement, 1.25 ml L-glutamine (200 mM), 5 ml penicillin–streptomycin, 484 ml neurobasal medium and filtering through the Stericup filtration system. Store the medium at 4 °C for up to 1 month and warm up to 37 °C before use.

Gelatin solution preparation

Prepare 10% (wt/vol) gelatin solution by mixing 10 g bovine skin gelatin powder with 100 ml deionized (DI) water (or DPBS) and leaving the mixture in a warm water bath at 37 °C overnight. Check if the gelatin has dissolved completely and the solution is homogeneous. If needed, the solution can be left in the warm water bath for 12 more hours. This solution can be stored in the fridge at 4 °C for up to 3 months and warmed up to 37 °C before use. Prepare aliquots to avoid multiple freeze–thaw cycles and prolonged exposure to heat.

▲ **CRITICAL** Gelatin can be very slow to dissolve and hence may take hours to make a homogenized solution.

Riboflavin solution

Prepare 0.1% (wt/vol) solution by dissolving 100 mg riboflavin powder in 100 ml DPBS. Riboflavin is light sensitive (both powder and solution), therefore preparing fresh solution for each application is recommended.

Glutaraldehyde solution

Prepare 0.5% (wt/vol) solution by mixing 0.5 ml of 70% glutaraldehyde stock solution with 69.5 ml DPBS. The stock solution should last 12 months at 4 °C. The 0.5% (wt/vol) working solution should be prepared fresh before application.

Oxaliplatin solution

Prepare a 5.0 mM stock solution of oxaliplatin chemotherapy drug by dissolving 5 mg oxaliplatin powder in 2.5 ml DPBS. The solution may need to the heated to 37 °C and sonicated for fast

dissolution. Dilute the stock solution 1:1,000 with culture medium to get a final concentration of 5 µM. Prepare fresh solution for each application.

Staining reagents

For all reagents used in staining, use freshly prepared working solution.

- Fixing solution: prepare 4% (wt/vol) PFA solution in PBS from stock solution of 16% (wt/vol) PFA
- Permeabilization solution: prepare stock solution of 10% (vol/vol) Triton X-100 by dissolving 5 ml Triton X-100 in 50 ml PBS. The solution may need to be sonicated for fast dissolution. Dilute the stock solution by 1:50 with PBS to prepare 0.2% (vol/vol) Triton X-100 solution
- Blocking solution: prepare stock solution of 10% (wt/vol) BSA by dissolving 5 g BSA in 50 ml PBS. Dilute the stock solution by 1:2 with PBS to prepare 5% (wt/vol) BSA solution. Then add the NGS stock solution (100%) to get a dilution of 1:20. The final blocking solution will contain 5% (vol/vol) BSA and 5% (vol/vol) NGS
- Staining solution: dilute the primary and secondary antibodies at different ratios in blocking solution

Procedures

Fabrication of the mold

● **TIMING 2–2.5 h**

▲ **CRITICAL** All steps in this procedure must be carried out in a microfabrication cleanroom. Chemicals and instrument required for this process are usually available in a standard fabrication cleanroom.

1. Clean a 4 inch single side polished 500-µm-thick silicon wafer with acetone, IPA and DI water. Then blow dry the wafer using a nitrogen gun.
   ▲ **CRITICAL STEP** This step is performed in a chemical fume hood.
2. Bake the wafer for 120 s on a hotplate at 110 °C for further dehydrating.
3. Place the wafer on the spinner, and spin coat with adhesion promoter AP8000 using a standard recipe (e.g., 500 rpm spread cycle for 10 s followed by a 30 s spin at 3,000 rpm for solvent drying).
4. Spin coat with SPR 220-4.5 positive photoresist (PR) using the same spinning recipe.
   - Note: a negative PR can also be used if the mask is designed accordingly
5. Soft bake the wafer for 180 s (120 s at 60 °C, then 60 s at 110 °C) on hotplates.
6. Properly place the design mask and PR-coated wafer in the mask aligner and expose to UV light with a dose of 160 mJ/cm^2.
   ▲ **CRITICAL STEP** Choose the appropriate contact mode between the mask and the wafer based on the minimum dimension in the design.
7. Develop the exposed wafer with AZ 400K (diluted 1:5 with DI water) for ~45 s. Rinse with DI water and blow dry with nitrogen.
8. Hard bake the wafer 120 s at 110 °C on a hotplate. The wafer is now ready for DRIE.
9. Etch the wafer in a DRIE machine (e.g., STS Pegasus ICP-DRIE) to achieve an etching depth of ~200 µm. Etching time is controlled to achieve the desired depth of the mold.
   ▲ **CRITICAL STEP** The etching depth may vary based on the machine, as well as the proportion of etching area on the wafer. Some iteration may be necessary to achieve the desired depth.
10. Strip the remaining PR off the wafer using Microposit Remover 1165, acetone and DI water. Blow dry with nitrogen.
11. (Optional) Clean the wafer by reactive-ion etching (RIE) process using oxygen and argon plasma in RIE-March Jupiter III.
    - Note: this step is optional, but highly recommended

12. Deposit a layer of PTFE on the wafer in a standard machine (e.g., Plasmatherm SLR 770). The mold should be ready to use. A 4 inch wafer can contain as many as ~100 sensors or even more.
    - Note: the thickness is not very critical, since this layer is to facilitate removal of the PDMS sensors from the mold

    ▲ **CRITICAL STEP** DO NOT use acetone on the mold after PTFE deposition since they will strip the coating off.

Fabrication of the sensors

● **TIMING 1–2 days**

13. In a plastic dish, pour PDMS (Sylgard 184) base and cross-linker at 10:1 ratio by weight and vigorously mix with a spatula.

    ▲ **CRITICAL STEP** The mixing should be done thoroughly so that the mixture becomes homogeneous. Bubble formation is normal at this step.
14. Remove the bubbles from the mixture by applying negative pressure for 30 min in a vacuum desiccator.

    ▲ **CRITICAL STEP** As the bubbles grow in volume in the desiccator, they may overflow the container if it is not large enough.
15. Very carefully pour small amounts of liquid PDMS in the molds on the silicon wafer using a fine pipette tip, e.g., a 10 µl pipette tip. Add the first droplet on base side of the mold and allow liquid PDMS to spread on its own. As the liquid reaches the beam channels, capillary tension will drive it toward every part of the mold. Add very small incremental amounts to the molds until the total depth is filled. Very carefully visualize the level of PDMS after each drop is added. Try tilting the wafer and looking from different angles to get a better view. Take special care to avoid overflow.

    ◆ **TROUBLESHOOTING**
16. After filling all the molds in the wafer with liquid PDMS, place the wafer in an oven at 60 °C for ~4–12 h. Place the wafer on a flat surface that is perfectly horizontal. A bubble level can be used to achieve this goal.
17. After curing and polymerization, the PDMS sensors are ready to be taken off the molds. Using a pipette, drop small amounts of IPA on the sensors in the molds and let sit for ~10 min.

    ▲ **CRITICAL STEP** IPA helps in peeling the sensors off the molds. Removal of the sensors without using IPA is also possible; however, this may result in breakage of thin elements in a few specimens.
18. Using fine tweezers, gently start lifting off the sensors from the base side and slowly work up to the spring beams and tissue grips. The whole sensors should come off the molds without any tears or damage.

    ▲ **CRITICAL STEP** This step should be conducted slowly and gently, otherwise several parts can break which may change the configuration of the sensor. However, the sensors are very robust and are only broken when excessive force is applied.

    ◆ **TROUBLESHOOTING**
19. To remove unreacted PDMS monomers, submerge the sensors in 70% (vol/vol) IPA and leave overnight.
20. Wash the sensors with DI water, and then autoclave to remove remaining IPA and sterilize.
    - Note: autoclaving can be done multiple times to ensure no toxic substance in present in PDMS
21. After sterilization, store the sensors in DI water or 70% (vol/vol) IPA.

    ■ **PAUSE POINT** Sensors can be stored for a long time in either water or IPA at room temperature (~20 °C) or in the refrigerator. Storing in IPA is preferred for ease of handling as PDMS is less sticky in IPA. If stored in IPA, the sensors must be cleaned before use to remove IPA. Perform cleaning by keeping the sensors in DI water at 60 °C in an oven for 2–3 days, changing water everyday. Also, autoclave multiple times if needed.

    ◆ **TROUBLESHOOTING**

Preparation of the experimental setup

● **TIMING 2.5–3 h**

22. Prepare a 10% (wt/vol) gelatin solution and leave in a warm water bath at 37 °C overnight.
23. Take the sensors out of DI water, place in a Petri dish with tweezers and let dry in a biosafety cabinet.
24. While the sensors are drying, stick double-sided tape to the bottom glass of a Petri dish, pour gelatin as shown in Fig. 3b and let it gel in the refrigerator for ~30 min. During the gelation process, gelatin also dries and shrinks. Hence, slightly overfill with liquid gelatin so that a flat substrate (as thick as the tape) can be achieved after gelation.
    - Tip: ensure that the gelatin completely solidifies and the top surface is dry, else the sensor will stick too much to gelatin reducing maneuverability. If required, keep in the refrigerator longer, without the lid on the Petri dish
25. Stick the sensor's base to the tape and place the beams and grips on the gelatin substrate as shown in Fig. 3b. Use a syringe needle to straighten the beams and position the grips at the correct locations.
    - Note: a microscope or at least a magnifying glass is required to perform this step
    - Tip: if the sensor sticks too much to gelatin, dry the gelatin more. Changing position of the sensor should leave minimal marking on gelatin, indicating proper surface dryness. Optimize drying time based on laboratory conditions
26. Using Noyes scissors, sever the connection between sensing springs and supporting beams (Fig. 3b).
    - Tip: cutting the connector may disturb the gelatin substrate. However, as long as these cuts and breaks are away from the tissue site between grips, they do not affect subsequent steps or results
27. Add gelatin to the sensor: for type I tissues follow option A, for type II follow option B and for type III follow option C. This step has to be carried out with the Petri dish under the microscope (e.g., Olympus IX81, Olympus IX51, stereo microscope, etc.).
    - Tip: microscope light should be minimized to avoid heating and drying of gelatin. Also, minimizing processing time is beneficial for avoiding drying

    (A) **Type I: for a single cell, a number of cells or a mixed coculture in all part of the tissue**

    (i) Using a needle, carve out two blocks of gelatin from the substrate and place them by the sides of the grips, as shown in Fig. 4a.
        - Tip 1: use a stiff needle with gauge number 22G or lower. Also, needles longer than 1 inch are helpful
        - Tip 2: it is not necessary to precisely control the size and shape of these gelatin blocks. The goal is to create a closed chamber between the grips. If the blocks are in contact with the outside of the grips, it is generally sufficient
        - Tip 3: it is helpful to secure these blocks using liquid gelatin as a glue. Dip the tip of the needle in liquid gelatin (in a separate container) and tap on the sides of the blocks. Liquid gelatin will solidify upon contact with cold blocks and make them stick to substrate and grips

        ◆ **TROUBLESHOOTING**

    (ii) Using a 20 µl pipette, pour liquid gelatin on the sensor beams and other parts of the sensor away from the grips (Fig. 4b). Use a needle to guide gelatin to every corner and pay close attention so that there are no air pockets.
        - Tip: this step should also be done under a microscope

        ▲ **CRITICAL STEP** This is the most critical step in the process. Pour a very small amount of gelatin at a time so that the grips are not inundated. The gelatin blocks previously placed help stop liquid gelatin from flowing into the grips. This gelatin layer solves a number of potential problems such as air bubbles, tissue rupture and stiction between beams.

        ▲ **CRITICAL STEP** Laboratory temperature should be at ~20–25 °C to allow enough time for maneuvering gelatin. Lower temperatures cause high viscosity and quick gelation, making it difficult to fill all the corners. At higher

temperatures, low viscosity makes gelatin flow faster, increasing the possibility of flooding the tissue site.

◆ TROUBLESHOOTING

(B) **Type II: for placing the cells in the grips and keeping the center free of cells**

(i) Using a needle, carve out a block of gelatin from the substrate and place it between the grips, as shown in Fig. 5a.

- Tip: the shape of this block is not important. However, make sure that the proper distance between grips is maintained. Too large a block may push the grips away from each other, which is not desirable. The goal is to occupy the space, so that cell–ECM cannot polymerize there

(ii) Proceed as directed in Step 27A(ii).

(C) **Type III: for two types of cells in two grips keeping the central portion devoid of cells**

(i) Proceed as directed in Step 27B(i).

(ii) Proceed as directed in Step 27A(ii).

(iii) Carve out another block of gelatin, and place it on top of one of the grips as shown in Fig. 6b.

- Tip: precise size and shape of this block is not necessary. However, secure this block at this location using liquid gelatin as described in Step 27A(i). Properly sticking these blocks ensures that they do not dislodge while performing next steps (particularly, bubble removal in vacuum desiccator)

Preparation of cell–ECM mixture and assembly of the tissue

● **TIMING 1.5–2 h**

28. Prepare a neutralizing solution (NS) by mixing 1 N sodium hydroxide, 10× PBS and DI water following Corning's recommended protocol[69]. For example, to prepare 500 µl 2 mg/ml final collagen solution from a stock solution with a concentration of 3.8 mg/ml, make NS by mixing 7.6 µl NaOH, 50 µl 10× PBS and 113.5 µl DI water. This 171.1 µl NS will be mixed with 328.9 µl collagen stock solution to prepare 500 µl working solution with 2 mg/ml final concentration (Step 31).
29. Fill up a crystalizing dish with crushed ice and place the collagen stock solution bottle, vial of NS and a few empty vials in the ice. Leave the container in the refrigerator until needed.
▲ **CRITICAL STEP** Most of the steps with collagen must be performed on ice, since collagen polymerizes very quickly at higher temperatures.
30. Trypsinize cells in the culture flask, centrifuge and aspirate the supernatant to get the cell pellet at the bottom of the tube.
    - Note: use cell-specific passaging protocols during this step
31. Put the cell containing tube in ice and mix collagen stock solution with NS on ice.
32. Mix the cells with the collagen solution by pipetting vigorously. For a single cell in the tissue, suspend the cells at a density of ~150×10^3 cells/ml. Cell density can be increased for higher number of cells in the tissue.
    - Note: take care not to form bubbles when mixing cells with collagen.
33. Based on the tissue structure, proceed with one of the following three options: for type I tissues follow option A, for type II follow option B and for type III follow option C.

(A) **Type I: for cells in all parts of the tissue**

(i) Using a 20 µl micropipette, add 5 µl of cell–collagen mixture on the tissue site and grips, as shown in Fig. 4b.

- Note: to ensure homogeneity, mix the cell–ECM suspension with the micropipette before each use as cells tend to settle to the bottom. To minimize variation between samples, maintain the same cell density and volume of the droplet dispensed (e.g., 5 µl). Use 150×10^3 cells/ml for a single cell and increase density linearly for more cells. Also, the gap between the grips should be kept the same to achieve a consistent tissue size

▲ **CRITICAL STEP** Remember to perform these steps with all the materials on ice, and from this point onward, all remaining activities involving cell–collagen mixture should be finished in ~5–7 min.

(ii) Apply negative pressure for ~20 s in a vacuum desiccator. This step facilitates removal of air pockets in the grips and allows the cell–collagen mixture to fill in the space.
- Note: keep ice packs in the desiccator to keep the temperature low

◆ **TROUBLESHOOTING**

(iii) Add some cell culture medium close to the dish walls, away from the sensor so that the tissue does not dry up while polymerizing.
- Note: adding medium is very important to keep the humidity in the Petri dish, maintain integrity of tissue structure and ensure good health of the cells

▲ **CRITICAL STEP** Do not add media to the tissue at this step.

(iv) Keep the Petri dish in a biosafety hood for 10–15 min at room temperature for collagen polymerization and tissue formation.
- Note: the polymerization temperature of collagen is a critical determinant of the matrix stricture; therefore, ensure that the same temperature (e.g., ~20 °C) is maintained for all experiments

▲ **CRITICAL STEP** It is not possible to raise the temperature to 37 °C for fast polymerization since gelatin melts at such temperature and causes collapse of the set up.

(B) **Type II: for cells in the grips, with central section free from cells**

(i) Proceed as directed in Step 33A(i). Refer to Fig. 5b.
- Tip: a very high cell density (~10 million/ml) works well for this type of sample. High density ensures that a large number of cells stick within the grips after the following steps. For consistency, keep the cells density constant for all replicates

(ii) Proceed as directed in Step 33A(ii).

(iii) Twine the corner of a Kim wipe and use it to remove excess cell–collagen mixture from the vicinity of the tissue location.
- Note: removal of excess cell–collagen mixture will not remove collagen and cells that occupied the inside of the grips, since they are locked inside
- Tip: allow some time (~5 min) for the cells to settle to the bottom. While waiting, keep some Kim wipes with twined corners ready to go. Some cells may get dislodged from the grips when removing excess cell–ECM. However, there should still be enough cells packed in the grips

▲ **CRITICAL STEP** This step should be finished as quickly as possible since collagen has already started to polymerize.

(iv) Using a 20 µl pipette, add small droplets (~5 µl) of collagen (without cells) at the tissue site and grips, as shown in Fig. 5c. Drops at the central region usually spreads to the grips and tissue location.

(v) Use a needle to quickly remove the gelatin block between the grips. The central portion of the tissue will now be occupied by collagen without cells.
- Tip: if some cells displace from the grips and land into the mid-section, it is possible to gently move them back into the grips

◆ **TROUBLESHOOTING**

(vi) Proceed as directed in Step 33A(iii).

(vii) Proceed as directed in Step 33A(iv).

(C) **Type III: for two types of cells in two grips keeping the central portion devoid of cells**

(i) Proceed as directed in Step 33A(i). Refer to Fig. 6c.
- Tip: a high cell density (~10 million/ml) works well for this step. It is important to secure the blocks in place using liquid gelatin

(ii) Proceed as directed in Step 33A(ii).

◆ **TROUBLESHOOTING**

(iii) Proceed as directed in Step 33B(iii).

(iv) Quickly remove the gelatin block placed on one of the grips using a needle.
- Tip: it is okay if the block breaks during removal with the needle. Guide the broken pieces away to open up the space within the grip

(v) Add a droplet of cell–collagen mixture containing another type of cells (Fig. 6d).
- Tip: use a high-density cell–ECM mixture

(vi) Repeat Step 33A(ii).
(vii) Repeat Step 33B(iii).
(viii) Repeat Step 33B(iv).
(ix) Repeat Step 33B(v).
(x) Proceed as directed in Step 33A(iii).
(xi) Proceed as directed in Step 33A(iv).

34. Gently add adequate amount of cold (4–8 °C) culture medium so that the sensors with assembled tissues are submerged in the medium and place the dish in the incubator.
    - Tip: be extra careful when adding media close to the tissue. Make a hanging droplet from the pipette tip and slowly lower the droplet to touch the tissue. Do not drop medium from height onto the tissue, as the slightest impact may damage the tissue
    ▲ **CRITICAL STEP** The temperature of the medium must be below 20 °C. Otherwise, if the medium is warm, it will dissolve gelatin quickly damaging the setup.
    ◆ **TROUBLESHOOTING**
35. After ~30–60 min, washout the medium (containing dissolved gelatin) and replace with fresh medium. Optionally, if the experiment requires, drugs can be applied by mixing with the media at this stage or afterward at any desired timepoint.
    ◆ **TROUBLESHOOTING**

Data acquisition and analysis

● **TIMING Flexible**

36. Place the Petri dish containing sensors (a 60 mm dish with 30 mm glass-bottom well can contain up to 8 sensors) on a motorized stage in an environment-controlled chamber enclosing an optical microscope (e.g., Olympus IX81) mounted on a vibration isolation table.
37. Set the temperature at 37 °C, CO_2 at 5% and humidity at 70%.
38. Set the locations and focal distances for all the tissues in the dish in the software (e.g., Metamorph) that controls the microscope and the stage. Also set the time interval for imaging.
39. Start image acquisition in phase contrast or brightfield mode using an objective with 20× magnification or higher.
    - Tip: if the image acquisition software is equipped with an auto-focus or focus correction feature (e.g., Zeiss Definite Focus), it is recommended to take advantage of it. This can help with correcting drift in the *z* axis and minimize noise in force readout, especially for long-term experiments
    ▲ **CRITICAL STEP** The initial 2 h of imaging can have problems with focusing, as the set up adjusts to the temperature changes. Keep an eye on the images and correct focus until it becomes stable.
    ◆ **TROUBLESHOOTING**
40. For calculating spring displacements (and force, $F = K_s \times d_c$.), analyze images of the sensor gauges (or the tissue grips) using the Template Matching plugin in ImageJ with subpixel resolution. Detailed instructions are provided below in the 'Image analysis with ImageJ' section and Supplementary Tutorial.

Tension–compression testing for stiffness measurement

● **TIMING 10–30 min**

▲ **CRITICAL** The initial stiffness should be measured immediately after gelatin is washed out (Step 35) so that the cells do not affect the matrix properties. Afterward, if assessing matrix remodeling by cells, measurements every 24 h are generally sufficient to determine remodeling by the cells.

41. Attach a needle to the *XYZ* linear stage and place it on the microscope stage, as shown in Fig. 4g.
    - Note: the micrometers in the *XYZ* linear motorized stage can either be manual or piezo-actuated. A piezo-actuated stage allows more control and precision; however, the manual stage also works

42. Using the stage and microscope, guide the needle through the hole in the stiff beam (see Fig. 1c to locate the access hole).
43. For the compression test, move the needle toward the tissue at a controlled rate (e.g., 10 µm/s worked well for our experiments), so that the stiff spring compresses the tissue. At the same time, keep imaging at a frequency commensurate with the rate of displacement. We suggest imaging frequency of 30 fps or higher.
44. Unload the sample by moving the needle away from the tissue.
45. For the tension test, keep moving the needle away from the tissue at a controlled rate so that the stiff beam starts to extend the tissue. Keep imaging during the whole process.
46. Unload the sample by moving the needle back to initial position, and then retract the needle.
47. (Optional) After force and stiffness data acquisition is complete (i.e., the final stiffness test after the duration of experiment), fix and stain the samples using standard immunohistochemistry procedures.

Image analysis with ImageJ

● **TIMING 5–10 min**

▲ **CRITICAL** The steps in this section instruct should be performed when analyzing tension–compression data. This data should provide tissue force and deformation, which can be used to determine the tissue stiffness.

48. Install the Template Matching and Slice Alignment plugins[70] on ImageJ.
49. Create a stack with all the images.
50. Rotate the images, if necessary, so that the grips and the tissue align with either the *x* or *y* axis.
51. Align the slices in the stack with respect to the grip connected to the stiff beam (see Supplementary Tutorial, pages 20–22). Select the analysis settings (e.g., matching method: normalized correlation coefficient, subpixel registration, bicubic interpolation for subpixel translation (see Supplementary Tutorial, page 21)) and choose the stiff grip as the region of interest (see Supplementary Tutorial, page 22, yellow box). All the slices should now be aligned with the stiff grip in a fixed location. Save the translation values in pixels and convert to microns (δ'_r).
52. Align the slices with respect to the soft grip by selecting the grip as the region of interest (see Supplementary Tutorial, page 25, yellow box). The analysis settings can be the same as in Step 51 (see Supplementary Tutorial, page 21). Save the translation values that give spring displacement in pixels.
53. Convert the displacement (δ_c) to microns, multiply with the spring constant to measure the force ($F = K_s \times \delta_c$). For the stiffness measurement procedure, the displacement (in microns) of the soft grip, as measured in Step 52, is denoted by δ'_c or δ'_t for compression or tension, respectively.
54. For measuring the stiffness, calculate force from $F'_c = K_s \times \delta'_c$ or $F'_t = K_s \times \delta'_t$ for compression and tension, respectively. Tissue deformation can be determined from following equations: $\Delta L'_c = \left(L'_c - L'_0\right) = \left(|\delta'_c| - |\delta'_r|\right)$ or $\Delta L'_t = \left(L'_t - L'_0\right) = \left(|\delta'_r| - |\delta'_t|\right)$, where δ_r and $\delta'_{(c\ or\ t)}$ are the displacements of stiff and soft grips, respectively. L'_0 and $L'_{(c\ or\ t)}$ are the initial (before actuation) and deformed tissue lengths, respectively. Additional instruction is provided in the Supplementary Tutorial.

(Optional) Secondary calibration of the spring constant, K_s

● **TIMING 10–30 min**

▲ **CRITICAL** Calibration of the sensor's spring constant should be performed just before preparing the experimental setup (i.e., before starting Step 22) or after the experiment is complete (i.e., after Step 46). In this case, however, the samples will need to be dissolved with collagenase (e.g., 100 U/ml collagenase type II, 12 h at 37° C) before calibration.

55. Attach a straight tungsten wire or fiber glass rod (e.g., the calibrator pins used in Fig. 2) to the *XYZ* linear stage and place it on the microscope stage, as shown in Fig. 4g.
    - Note: this cantilever rod, with known material and geometric properties, functions as the calibrating beam. Choose the length (L_c) of the calibrator such that the calibrator

stiffness, $K_c = \frac{3E_cI_c}{L_c^3} \approx \frac{12nEI}{L^3} = K_s$, so that both the spring and the calibrator undergoes similar deformations. Here, E_c and I_c are modulus of elasticity of the calibrator's material and moment of inertia ($I_c = \pi D^4/64$, with D being the diameter), respectively. Also, it is important that the calibrator beam is vertical so that it is perpendicular to the spring axis

56. Using the linear stage, move the calibrator beam so that the bottom tip is sticking to the grip connected to the soft spring.
    - Note: the process is similar to the one shown in Fig. 2c, except that the tip of the calibrator is sticking to the soft grip (and the space between grips is empty without tissue or matrix)
57. Move the top end of the calibrator by δ_{a1} (e.g., ~10 µm) in the direction of the spring and take an image of the grip. From the image, determine the displacement of the spring (δ_{s1}) and the bottom end of the calibrator ($\delta_{b1} = \delta_{a1} - \delta_{s1}$).
58. Increase the displacements to δ_{a2} (e.g., ~20 µm), δ_{s2} and δ_{b2}.
59. Determine the average spring constant, $K_s = \frac{\sum_{i=1}^{n} K_{si}}{n}$, where $K_{si} = \frac{K_b\delta_{bi}}{\delta_{si}}$, ($I = 1, 2, 3, 4, \ldots \ldots \ldots$).

Troubleshooting

Troubleshooting advice can be found in Table 2.

Table 2 | Troubleshooting table

Step	Problem	Possible reason	Solution
15	Overfilling the molds while pouring PDMS	Thick pipette tip	Use a thin pipette tip and add droplets from the base side
18	Thin components of the sensors break when taking out from the molds	Inadequate PTFE coating	Increase the PTFE deposition time in Step 12
			Increase time for IPA absorption in Step 17
			Be gentle and slow when pulling the soft parts out
21	Sensor beams sticking to each other while storing	PDMS has high adhesion	For long term storage, keep the sensors in 70% (vol/vol) IPA. IPA helps keep the sensor beams separate and straight. Clean by keeping the sensors in DI water at 60 °C in an oven for 2–3 days, changing water every day. Also, autoclave multiple times, if needed
27	Gelatin dries out while setting up the device	Evaporation due to microscope light	Try using lower light intensity to reduce loss of moisture
27A(i)	Gelatin blocks disintegrate while handling	Inadequate gelation time	Allow longer time for gelation and drying in Step 24. Also, the blocks do not need to be in a particular shape as long as they are creating a barrier at the sides of the grips
	Gelatin blocks not sticking to the grips	Excessive dehydration of gelatin	Use a shorter gelation period or add a little DI water to the needle before cutting gelatin blocks
27A(ii)	Gelatin getting into the grips and the site for tissue	Low viscosity of gelatin	Try using gelatin at a slightly lower temperature than 37 °C. Also, keep a cold pack nearby so that gelatin can be flash frozen if it is about to flow into the grips
33	Collagen polymerizing too quickly	High room temperature	All components of the experimental setup should be kept on ice. Also, keeping some cold packs in the vacuum desiccator helps keep it cold
33A(ii)	The tissue does not contain desired number of cell(s)	Sub-optimal cell density	Alternative method: proceed to finish Step 33A(ii) (i.e., addition of cell–ECM and suction for bubble removal). At this stage, check if the desired number of cells landed on the target region. If not, gently use a twined kimwipe to remove the cell–ECM from the tissue site, and add fresh mixture. Repeat this process until the desired number of cells land in the tissue
33B(v)	Difficulties in removal of the gelatin block	High stiction and softness of gelatin	Use a small PDMS block for easy removal
33C(ii)	Same type of cells in both grips	Movement of gelatin blocks during vacuum application	Twist a corner of a kimwipe to make a sharp end. Use the pointed end of the kimwipe to remove unwanted cells from within the grip. Removal of cells from one grip should not affect cells in the other grip, since those cells should be firmly placed
34	Prongs of the grips closing in	Swelling of gelatin with absorption	Place the gelatin blocks slightly away from the grips' outside prongs. This space will allow gelatin to expand without pushing the grip prongs inside
35	Bubbles forming between the beams and close to the tissue	Bubbles trapped in gelatin	Try removing the bubbles from gelatin before it gels, using a needle. If this does not work, perform washout with PBS several times. If this method does not work, follow the next instruction. After polymerization of the tissue, submerge the setup with cold PBS (4–8 °C) and apply negative pressure for 30 s in the vacuum. Finally, replace the PBS with cold culture medium and put the dish in the incubator

Table 2 (continued) | Troubleshooting table

Step	Problem	Possible reason	Solution
39	Change of focus during image acquisition	Conditions of the environment chamber not stable	Turn on the heater, CO_2 and the humidifier for the environment chamber for 15 min before the formation of tissues. Also, put the Petri dish containing the sensors and tissues ~30 min in the chamber for stabilizing before starting imaging
	Unhealthy cells in the tissue	Toxicity from PDMS monomers or residual IPA	Leave the sensors in DI water at 60 °C in an oven for 2–3 days, changing water everyday. Alternatively, single autoclaving can remove most of the unwanted toxic elements. Note that autoclaving may induce permanent deformation of the beams if not placed in its natural shape. Make sure that the beams are separate and straight before placing in the autoclave
	Tissue detaching from grips	Mechanical anchorage is not sufficient, chemical treatment required	After making the sensors, perform the following surface modification before Step 22: (1) coat the sensors with 2% (vol/vol) 3-aminopropyl)trimethoxysilane in ethanol for 12 h, (2) wash with ethanol for 1 h, (3) wash 3× with water, (4) coat the sensors with 0.5% (wt/vol) glutaraldehyde in water for 1 h, (5) wash 3× with water

Timing

Steps 1–12, Fabrication of the mold: 2–2.5 h
Steps 13–21, Fabrication of the sensor: 1–2 days
Step 22: Preparation of gelatin solution: 8 h
Steps 23–27, Preparation of experimental setup: 2.5–3 h
Steps 28–35, Preparation of cell–ECM mixture, and assembly of the tissue: 1.5–2 h
Steps 36–39, Data acquisition: 1–72 h, as required
Step 40, Data analysis: 10–30 min
Steps 41–47, Stiffness measurement: 10–30 min
Steps 48–54, Image analysis: 5–10 min
Steps 55–59, Calibration: 10–30 min

Anticipated results

We demonstrate that following the procedure, we can construct tissues with various configurations and measure cell/tissue force and stiffness. Figure 7 shows three distinct types of tissues for different assays. We define these three types as type I: tissue with single or multiple cell(s) in the tissue (Fig. 4); type II: similar cells inside the grips with the central region free of cells (Fig. 5); and type III: different types of cells in two grips keeping the central portion without cells (Fig. 6). Figure 7a–f (adapted from ref. 34) shows a cancer model with cancer and stromal cells in the tissue (type I). The confocal images show that the model consists of one FET (human colon cancer cell line) cluster, a few CAF05 (human colon) fibroblasts and collagen as ECM. Confocal *z*-stack images of F-actin/nuclei labeled cells and two-photon second harmonic generation (SHG) images of collagen were used to reconstruct the 3D tissue structure (Fig. 7d–f). Figure 7g,h show models for type II tissues, where mouse primary neurons and glial cells are placed in the grips and the central region is ECM without cells. Astrocytes and neurons were stained with specific markers that show high-density clusters of cells within grips and neurites in the central region (Fig. 7g). Live brightfield and fluorescence imaging of F-actin (labeled with SiR-Actin) shows that the cells extend neurites (axons and/or dendrites) through the tissue and create connections (Supplementary Videos 2 and 3, adapted from Joy et al.[26]) We also confirmed formation of mature synapses in the 3D tissues. Immunostaining with neurite (MAP2), pre- and postsynaptic (Bassoon and Homer) markers, we show that pre- and postsynaptic markers are colocalized, revealing synaptic connections on the sensor (Fig. 7h, adapted from ref. 26). Figure 7i,j present two examples of type III tissues: cancer cells in one grip CAFs in the other. In Fig. 7i, we demonstrate a low density of cells and Fig. 7j exhibits a tissue with high number of cells. Interestingly, by keeping cancer and stromal cells at a distance, this type of tissue allows creating a gradient of secreted factors and mechanical cues such as strain and

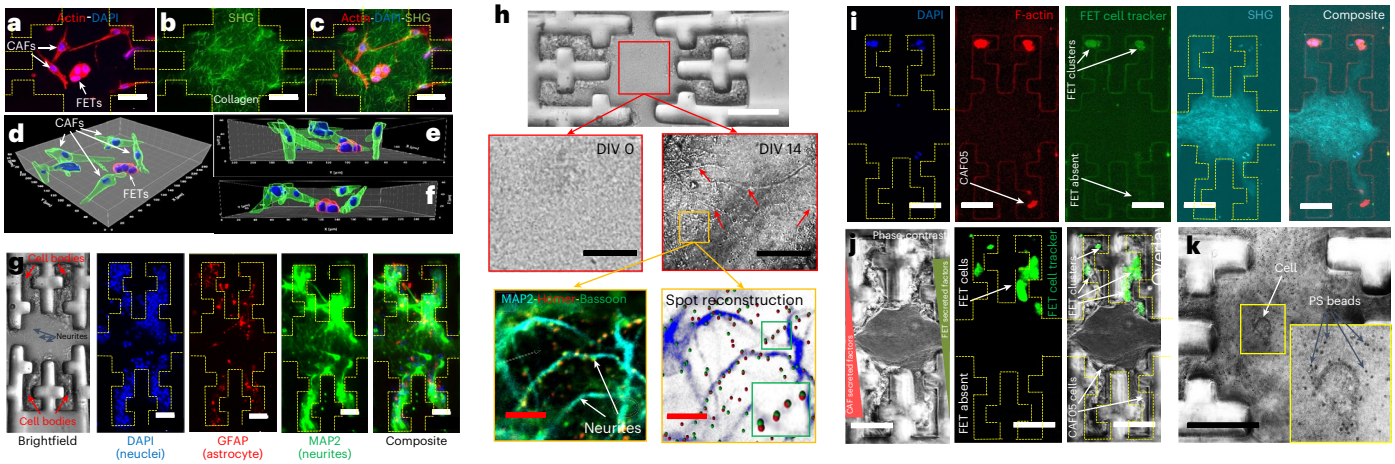

Fig. 7 | Various examples of tissues on the sensor. a–**f**, Type I tissue: a 3D tumor model with cancer and stromal cell coculture. F-actin and nuclei labeled with phalloidin and DAPI, respectively (**a**); an SHG image of collagen scaffolds (**b**); an overlay of phalloidin, DAPI and SHG (**c**); 3D surface rendering of confocal *z*-stacks of F-actin (phalloidin) and nuclei (DAPI) of the cells (**d**); and the *XZ* (**e**) and *YZ* (**f**) plane of the 3D rendered surface from **d**. **g**, For type II tissue with primary rat hippocampal neurons, a brightfield image shows the cell body clusters inside the grips and network of neurites at the middle region; immunofluorescence images show the nucleus (DAPI), astrocyte (GFAP), neurite (MAP2) and their composite. **h**, For type II tissue with primary rat hippocampal neurons, a brightfield and immunofluorescence (neurite marker MAP2 (cyan), presynaptic marker Bassoon (green), and postsynaptic marker Homer (red)) images show growth of neurites (indicated by arrow) after 14 days in vitro (DIV). The corresponding IMARIS spot reconstruction confirms the colocalization of pre- and postsynaptic markers and formation of mature synapses. **i**, Type III tissue with low cell densities of FET in one grip and CAF05 in the other. DAPI and F-actin staining locate all cells, while cell tracker only traces FET cancer cells. Hence, we can ascertain that the clusters in the top grip are FETs and the single cell in the bottom grip is a CAF05. **j**, Type III tissue with high cell densities. This tissue has a large number of FETs in the top grip and a few CAF05s in the bottom grip. The central region is free from cells. **k**, Tissue with PS beads for tracking ECM deformation. Black arrows indicate toward PS beads. In **a**–**g** and **i**, scale bars, 50 µm. In **h**, scale bars: white, 100 µm; black, 30 µm; red, 10 µm. In **j** and **k**, scale bars, 100 µm. The images in **a**–**f** were adapted with permission from ref. 34, AAAS. The image in **h** was adapted with permission from ref. 26, PNAS.

matrix density. This feature makes the sensor a convenient tool for investigating biophysical activities in 3D. Figure 7k demonstrates that beads can be added to the ECM, which may help monitor deformation of the matrix.

Figure 8a shows force data from single fibroblasts (CAF05) that are in a type I setup (Fig. 4). Phase-contrast images of the cells were also collected during the experiments. Representative images of the cells at different timepoints are also shown. The data present force dynamics of each CAF and highlight the common trends and heterogeneities between cells. For example, sample 3 shows a large increase in force at ~16 h, and this event was accompanied by excessive elongation of the cell (see phase-contrast images). Also, force curves from samples 1 and 2 show two different trends. The cell in sample 1 gradually increased its force without major relaxation at any point, while cell 2 shows a periodic increase and decrease in force. It can be anticipated that the cells exhibited different functions and signaling corresponding to the cellular force.

To establish clinical relevance, we showed that the sensor can host tissue with human patient-derived primary cells that can be used for personalized drug screening. CAFs were extracted and sorted from a primary colon tumor that was clinically diagnosed as an invasive moderately differentiated adenocarcinoma. Figure 8b shows data with these PrCAFs (see also Supplementary Video 4). Interestingly, these cells are highly contractile compared with the CAF05 cell line (human colon CAF). The traditional chemotherapy drug oxaliplatin was administered on the cells at 17 h at a concentration of 5 µM (ref. 71). The drug was not effective in reducing force generation of the cells. This result might indicate that the drug does not affect the stromal cells' contractility. By assembling the sensors in a high-throughput array, we could possibly perform clinical assays with a range of drugs and concentrations to assess the efficacy and optimal dosage for a particular patient. Most importantly, the data from the sensor is free from the artifacts of 2D culture. Therefore, this protocol shows prospects of developing into a novel method for personalized drug/phenotypic screening.

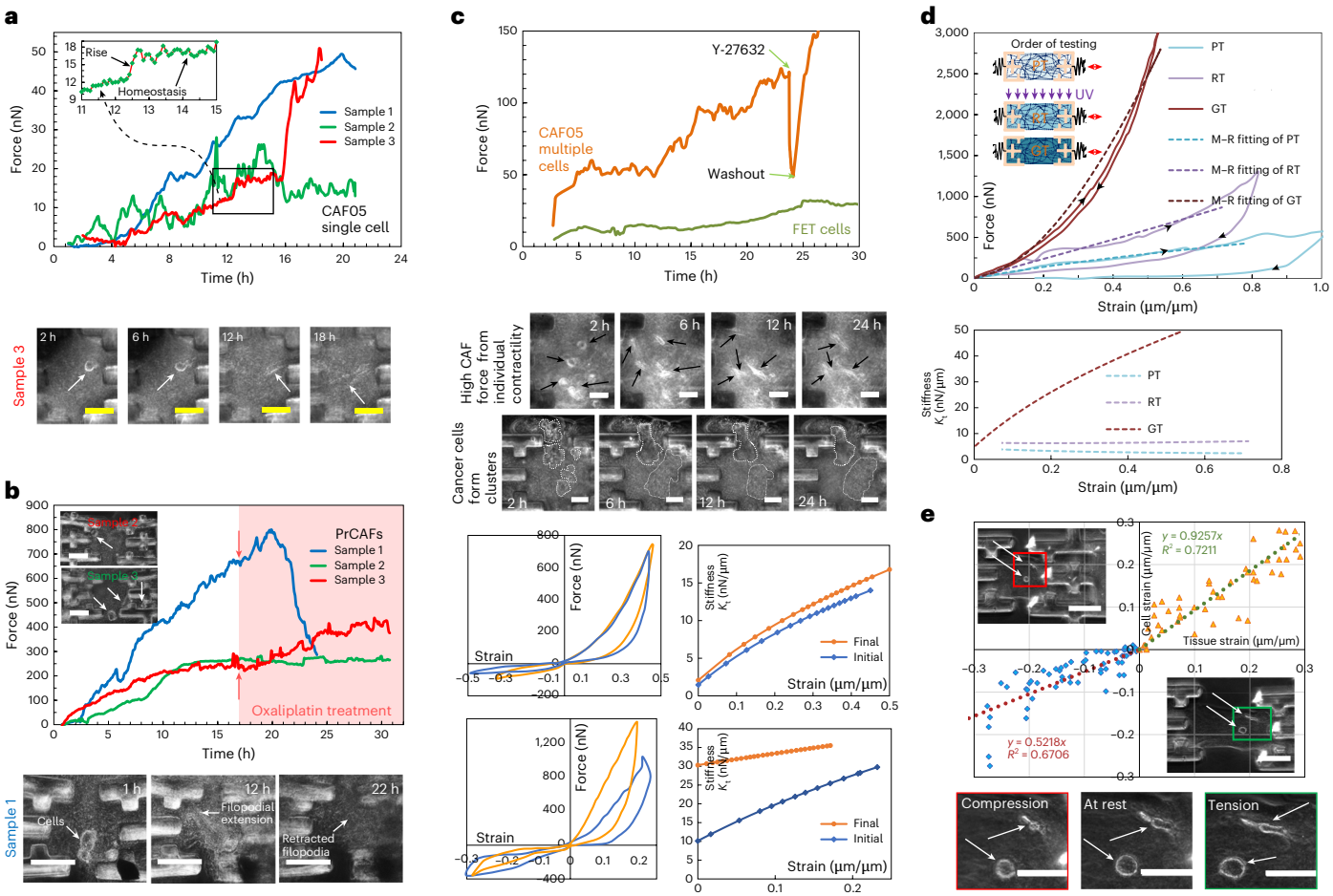

Fig. 8 | Application of the sensor for measurement of cell force, tissue stiffness and cell stretching. a, Traction force evolution of single CAF05 fibroblasts. The inset shows an enlarged portion of sample three data points taken every 5 min. Phase contrast images show the cell in sample 3. **b**, Cell force dynamics for PrCAF cells with oxaliplatin (chemotherapy drug) treatment. Phase-contrast images show that the cells are more contractile when elongated (sample 1). As the cells retract filopodia, cell force tends to decrease (Supplementary Video 4). Also, the drug apparently does not affect cellular traction generation for stromal CAFs. **c**, Force and ECM remodeling by multiple CAF05 and FET cells (both monocultures). CAF05 generates higher force compared with FET cancer cells. Stiffness tests were performed for the specimens at initially (2 h) and final timepoints (24 h for CAF05s and 40 h for FETs). Force–strain curves are shown for both initial and final tests. Tangential tensile stiffness was measured from Mooney–Rivlin fitting of the force-strain curves. FET specimen exhibits substantial stiffening, while CAF05 specimen shows slight increase of stiffness. Black arrows indicate cells. **d**, The sensor detects stiffness change of collagen with chemical cross-linking by RT and GT. RT increased the stiffness by 2–3-fold, while GT stiffened the tissue by ~7-fold at 50% strain. Mooney–Rivlin (M–R) fitting of the loading curves are shown in dashed lines. Plots for the slopes of the M–R curves indicate the tissue stiffness (bottom). **e**, Cell (CAFs) stretch–contraction test results on the sensor. The orange and blue markers represent tension and compression data points respectively. The linear regression lines for the data show the relationship between applied tissue strain and corresponding cell strain. The phase contrast images and the insets show the CAFs at different stages of the experiment—compressed, at rest and elongated. The white arrows indicate the location of the cells in the tissues. Scale bars, 100 μm. Images **a** and **c** were adapted with permission from ref. 34, AAAS.

We also created tissues with either multiple CAFs (CAF05) or multiple cancer cells (FETs) (type I setup) to show collective force evolution (Fig. 8c). As expected, CAFs are more contractile than cancer cells. Also, CAFs migrate and generate force as individual entities, while the FETs exhibit epithelial behavior by coalescing into large clusters and pull the ECM generating force. CAF force was inhibited with Y-27632 is indeed generated by cell contractility. In addition to force, we measured ECM remodeling by the cells by performing stiffness tests performed at the start and end of the experiments. For both CAFs and FETs, force–strain curves show non-linearity. The tensile loading data were fitted to the Mooney–Rivlin model and the tangent

tensile stiffness was measured from the model (Fig. 8c). The CAF sample had a very small increase in stiffness, but the FET sample shows substantial stiffening of the tissue.

It is known that the cell-induced matrix remodeling has two mechanistic sources: (i) fiber alignment due to cell force and (ii) chemical cross-linking and ECM deposition by cells. We wanted to show that the sensor is capable of detecting remodeling from cross-linking alone. To this end, we made collagen tissues without cells and chemically modified collagen tissue in two steps: first by riboflavin–UV treatment (RT)[72,73] and then by glutaraldehyde treatment (GT)[74,75]. RT was performed following Dresden protocol[76,77] (used for corneal collagen cross-linking as a treatment of keratoconus) and GT was done with 0.5% (wt/vol) concentration for 24 h (ref. 78). Figure 8d shows the stiffness of collagen before and after treatment. Interestingly, for pretreatment (PT) and RT conditions, the sample showed linear force–strain relationship and constant stiffness. However, RT increased the stiffness by ~2-fold. Remarkably, GT resulted in a major transformation. The sample exhibited non-linear behavior with substantial strain hardening. At low strains, the stiffness is similar to the PT or RT sample, but at higher strains, stiffness is substantially higher. For example, at 50% strain, the stiffness was increased by ~7-fold, compared with RT.

Utilizing the sensor, we also applied stretch and compression to the tissue (comprised of collagen I and CAFs) by applying a prescribed motion on the supporting spring using a piezo stage. The ECM is thus subjected to tensile and compressive strains, which transfers the strains to the cell. Figure 8e shows phase-contrast images of cells under stretch and contraction, and the relationship between cell and ECM deformation. Projected cell strain and ECM strain is quantified from the following –

$$\text{Cellstrain} = (\text{stretched length} - \text{resting length})/(\text{resting length}), \text{and}$$

$$\text{ECMstrain} = (\text{grid gap under stretch} - \text{grid gap at rest})/(\text{grid gap at rest}).$$

The data suggest that the cell strain is ~93% of the tissue strain in tension and 52% in compression. One explanation is that the cell gets stretched by the collagen due to cell–ECM adhesion. Under compression, fiber buckling reduces force and strain transmission to the cells. Readers should be careful in measurement and interpretation of cell strains from phase-contrast or brightfield images, since the data are projected on a plane. Such projected image provides partial information. Tomographic imaging techniques such as confocal microscopy should be used for accurately determining the 3D strains.

Data availability

All source data needed to validate findings in the protocol is available in the primary research papers and the Supplementary Materials of this paper. Any additional data related to this protocol may be requested from the authors. Source data are provided with this paper.

Received: 21 December 2023; Accepted: 8 November 2024;

References

1. Sakar, M. S. et al. Cellular forces and matrix assembly coordinate fibrous tissue repair. *Nat. Commun.* **7**, 11036 (2016).
2. Li, B. & Wang, J. H.-C. Fibroblasts and myofibroblasts in wound healing: force generation and measurement. *J. Tissue Viability* **20**, 108–120 (2011).
3. Handorf, A. M., Zhou, Y., Halanski, M. A. & Li, W.-J. Tissue stiffness dictates development, homeostasis, and disease progression. *Organogenesis* **11**, 1–15 (2015).
4. Zanotelli, M. R. & Reinhart-King, C. A. in *Advances in Experimental Medicine and Biology* Vol. 1092 (eds Dong, C., Zahir, N. & Konstantopoulos, K.) 91–112 (Springer, 2018).
5. Hadden, W. J. et al. Stem cell migration and mechanotransduction on linear stiffness gradient hydrogels. *Proc. Natl Acad. Sci. USA* **114**, 5647–5652 (2017).
6. Li, S., Huang, N. F. & Hsu, S. Mechanotransduction in endothelial cell migration. *J. Cell. Biochem.* **96**, 1110–1126 (2005).
7. Emon, B., Bauer, J., Jain, Y., Jung, B. & Saif, T. Biophysics of tumor microenvironment and cancer metastasis—a mini review. *Comput. Struct. Biotechnol. J.* **16**, 279–287 (2018).
8. Broders-Bondon, F., Ho-Bouldoires, T. H. N., Fernandez-Sanchez, M. E. & Farge, E. Mechanotransduction in tumor progression: the dark side of the force. *J. Cell Biol.* **217**, 1571–1587 (2018).
9. Wei, S. C. & Yang, J. Forcing through tumor metastasis: the interplay between tissue rigidity and epithelial–mesenchymal transition. *Trends Cell Biol.* **26**, 111–120 (2016).
10. Shakya, K. M., Noyes, A., Kallin, R. & Peltier, R. E. Evaluating the efficacy of cloth facemasks in reducing particulate matter exposure. *J. Expo. Sci. Environ. Epidemiol.* **27**, 352–357 (2017).

11. Bauer, J. et al. Increased stiffness of the tumor microenvironment in colon cancer stimulates cancer associated fibroblast-mediated prometastatic activin A signaling. *Sci. Rep.* **10**, 1–11 (2020).
12. Emon, B. et al. Mechanosensitive changes in the expression of genes in colorectal cancer-associated fibroblasts. *Sci. Data* **10**, 350 (2023).
13. Hanahan, D. & Coussens, L. M. Accessories to the crime: functions of cells recruited to the tumor microenvironment. *Cancer Cell* **21**, 309–322 (2012).
14. Karagiannis, G. S. et al. Cancer-associated fibroblasts drive the progression of metastasis through both paracrine and mechanical pressure on cancer tissue. *Mol. Cancer Res.* **10**, 1403–1418 (2012).
15. Kumar, S. & Weaver, V. M. Mechanics, malignancy, and metastasis: the force journey of a tumor cell. *Cancer Metastasis Rev.* **28**, 113–127 (2009).
16. Bissell, M. J., Hall, H. G. & Parry, G. How does the extracellular matrix direct gene expression? *J. Theor. Biol.* **99**, 31–68 (1982).
17. Bauer, J. et al. Increased stiffness of the tumor microenvironment in colon cancer leads to an increase in activin and metastatic potential. *Cancer Res.* **78** (Suppl. 13), abstr. 177 (2018).
18. Vogel, V. Mechanotransduction involving multimodular proteins: converting force into biochemical signals. *Annu. Rev. Biophys. Biomol. Struct.* **35**, 459–488 (2006).
19. Emon, B. & Saif, M. T. A. A window into solid stresses within tumours. *Nat. Biomed. Eng.* **7**, 1348–1349 (2023).
20. Nia, H. T. et al. Solid stress and elastic energy as measures of tumour mechanopathology. *Nat. Biomed. Eng.* **1**, 0004 (2016).
21. Zhang, S. et al. Intravital measurements of solid stresses in tumours reveal length-scale and microenvironmentally dependent force transmission. *Nat. Biomed. Eng.* **7**, 1473–1492 (2023).
22. Siechen, S., Yang, S., Chiba, A. & Saif, T. Mechanical tension contributes to clustering of neurotransmitter vesicles at presynaptic terminals. *Proc. Natl Acad. Sci. USA* **106**, 12611–12616 (2009).
23. Yuan, Z. et al. Extracellular matrix remodeling in tumor progression and immune escape: from mechanisms to treatments. *Mol. Cancer* **22**, 1–42 (2023).
24. Emon, B. et al. Nuclear deformation regulates YAP dynamics in cancer associated fibroblasts. *Acta Biomater.* **173**, 93–108 (2024).
25. Doha, U. et al. Disorder to order transition in cell–ECM systems mediated by cell–cell collective interactions. *Acta Biomater.* **154**, 290–301 (2022).
26. Joy, M. S. H. et al. Synapses without tension fail to fire in an in vitro network of hippocampal neurons. *Proc. Natl Acad. Sci. USA* **120**, e2311995120 (2023).
27. Sun, P. et al. Maintenance of primary hepatocyte functions in vitro by inhibiting mechanical tension-induced YAP activation. *Cell Rep.* **29**, 3212–3222.e4 (2019).
28. Goffin, J. M. et al. Focal adhesion size controls tension-dependent recruitment of α-smooth muscle actin to stress fibers. *J. Cell Biol.* **172**, 259–268 (2006).
29. Paszek, M. J. et al. Tensional homeostasis and the malignant phenotype. *Cancer Cell* **8**, 241–254 (2005).
30. McBeath, R., Pirone, D. M., Nelson, C. M., Bhadriraju, K. & Chen, C. S. Cell shape, cytoskeletal tension, and rhoa regulate stem cell lineage commitment. *Dev. Cell* **6**, 483–495 (2004).
31. Ahmed, W. W., Williams, B. J., Silver, A. M. & Saif, T. A. Measuring nonequilibrium vesicle dynamics in neurons under tension. *Lab Chip* **13**, 570–578 (2013).
32. Grashoff, C. et al. Measuring mechanical tension across vinculin reveals regulation of focal adhesion dynamics. *Nature* **466**, 263–266 (2010).
33. Porazinski, S. et al. YAP is essential for tissue tension to ensure vertebrate 3D body shape. *Nature* **521**, 217–221 (2015).
34. Emon, B. et al. A novel method for sensor-based quantification of single/multicellular force dynamics and stiffening in 3D matrices. *Sci. Adv.* **7**, eabf2629 (2021).
35. Elhebeary, M., Emon, M. A. B., Aydin, O. & Saif, M. T. A. A novel technique for in situ uniaxial tests of self-assembled soft biomaterials. *Lab Chip* **19**, 1153–1161 (2019).
36. Legant, W. R. et al. Microfabricated tissue gauges to measure and manipulate forces from 3D microtissues. *Proc. Natl Acad. Sci.* **106**, 10097–10102 (2009).
37. Schwarz, U. S. & Soiné, J. R. D. Traction force microscopy on soft elastic substrates: a guide to recent computational advances. *Biochim. Biophys. Acta Mol. Cell Res.* **1853**, 3095–3104 (2015).
38. Knoll, S. G., Ali, M. Y. & Saif, M. T. A. A novel method for localizing reporter fluorescent beads near the cell culture surface for traction force microscopy. *J. Vis. Exp.* https://doi.org/10.3791/51873 (2014).
39. Zhang, M. et al. A detailed protocol for cell force measurement by traction force microscopy. *Smart Mater. Med.* **5**, 106–113 (2024).
40. Kong, H. J., Polte, T. R., Alsberg, E. & Mooney, D. J. FRET measurement of cell-traction forces and nano-scale clustering of adhesion ligands varied by substrate stiffness. *Proc. Natl Acad. Sci. USA* **102**, 4300–4305 (2005).
41. Tan, J. L. et al. Cells lying on a bed of microneedles: an approach to isolate mechanical force. *Proc. Natl Acad. Sci. USA* **100**, 1484–1489 (2003).
42. Stout, D. A. et al. Mean deformation metrics for quantifying 3D cell–matrix interactions without requiring information about matrix material properties. *Proc. Natl Acad. Sci. USA* **113**, 2898–2903 (2016).
43. Steinwachs, J. et al. Three-dimensional force microscopy of cells in biopolymer networks. *Nat. Methods* **13**, 171–176 (2016).
44. Afthinos, A. et al. Migration and 3D traction force measurements inside compliant microchannels. *Nano Lett.* **22**, 7318–7327 (2022).
45. Piotrowski, A. S., Varner, V. D., Gjorevski, N. & Nelson, C. M. Three-dimensional traction force microscopy of engineered epithelial tissues. *Methods Mol. Biol.* **1189**, 191–206 (2015).
46. Emon, M. A. B. et al. Dose-independent threshold illumination for non-invasive time-lapse fluorescence imaging of live cells. *Extreme Mech. Lett.* **46**, 101249 (2021).
47. Blackmon, R. L. et al. Imaging extracellular matrix remodeling in vitro by diffusion-sensitive optical coherence tomography. *Biophys. J.* **110**, 1858–1868 (2016).
48. Chang, J.-K. et al. Cytotoxicity and in vitro degradation kinetics of foundry-compatible semiconductor nanomembranes and electronic microcomponents. *ACS Nano* **12**, 9721–9732 (2018).
49. Loverde, J. R. & Pfister, B. J. Developmental axon stretch stimulates neuron growth while maintaining normal electrical activity, intracellular calcium flux, and somatic morphology. *Front. Cell. Neurosci.* **9**, 308 (2015).
50. Wong, T.-Y. et al. Mechanical stretching simulates cardiac physiology and pathology through mechanosensor piezo1. *J. Clin. Med.* **7**, 410 (2018).
51. Sun, L. et al. Effects of mechanical stretch on cell proliferation and matrix formation of mesenchymal stem cell and anterior cruciate ligament fibroblast. *Stem Cells Int.* **2016**, 9842075 (2016).
52. Liu, M., Tanswell, A. K. & Post, M. Mechanical force-induced signal transduction in lung cells. *Am. J. Physiol.* **277**, 667–683 (1999).
53. Reid, S. E. et al. Tumor matrix stiffness promotes metastatic cancer cell interaction with the endothelium. *EMBO J.* **36**, 2373–2389 (2017).
54. Richard, M. N., Deniset, J. F., Kneesh, A. L., Blackwood, D. & Pierce, G. N. Mechanical stretching stimulates smooth muscle cell growth, nuclear protein import, and nuclear pore expression through mitogen-activated protein kinase activation. *J. Bio. Chem.* **282**, 23081–23088 (2007).
55. Friedrich, O. et al. Stretch in focus: 2D inplane cell stretch systems for studies of cardiac mechano-signaling. *Front. Bioeng. Biotechnol.* **7**, 55 (2019).
56. Atcha, H. et al. A low-cost mechanical stretching device for uniaxial strain of cells: a platform for pedagogy in mechanobiology. *J. Biomech. Eng.* **140**, 81005–81006 (2018).
57. Kamble, H., Barton, M. J., Jun, M., Park, S. & Nguyen, N. T. Cell stretching devices as research tools: Engineering and biological considerations. *Lab Chip* **16**, 3193–3203 (2016).
58. Kreutzer, J. et al. Pneumatic unidirectional cell stretching device for mechanobiological studies of cardiomyocytes. *Biomech. Model. Mechanobiol.* **19**, 291–303 (2020).
59. Hu, Y. et al. DNA-based ForceChrono probes for deciphering single-molecule force dynamics in living cells. *Cell* **187**, 3445–3459.e15 (2024).
60. Xu, F. et al. Quantum-enhanced diamond molecular tension microscopy for quantifying cellular forces. *Sci. Adv.* **10**, eadi5300 (2024).
61. Chopra, A. K. *Dynamics of Structures* 4th edn (Prentice Hall, 2011).
62. Beer, F. P., Johnston, E. R., DeWolf, J. T. & Mazurek, D. F. *Mechanics of Materials* (McGraw-Hill, 2006).
63. American Institute of Steel Construction. *Manual of Steel Construction: Allowable Stress Design* (American Institute of Steel Construction, 1989).
64. Crandall, S. H., Dahl, N. C. & Lardner, T. J. *An Introduction to the Mechanics of Solids* (McGraw-Hill, 2012).
65. Popov, E. P. *Engineering Mechanics of Solids* (Prentice Hall, 1998).
66. Ali, M. Y., Anand, S. V., Tangella, K., Ramkumar, D. & Saif, T. A. Isolation of primary human colon tumor cells from surgical tissues and culturing them directly on soft elastic substrates for traction cytometry. *J. Vis. Exp.* https://doi.org/10.3791/52532 (2015).
67. CD326(EpCAM) microbeads (human). *Miltenyi Biotec* http://www.ulab360.com/files/prod/manuals/201603/28/596760001.pdf (2007).
68. Pacifici, M. & Peruzzi, F. Isolation and culture of rat embryonic neural cells: a quick protocol. *J. Vis. Exp.* https://doi.org/10.3791/3965 (2012).
69. Certificate of analysis for Corning collagen I high concentration (HC), Rat Tail. *Corning Incorporated* https://certs-ecatalog.corning.com/life-sciences/certs/354236/354236_6207007.pdf (2013).
70. Tseng, Q. Template matching and slice alignment—ImageJ plugins. *ImageJ Plugins by Qingzong TSENG* https://sites.google.com/site/qingzongtseng/template-matching-ij-plugin#publications (2011).
71. Fujie, Y. et al. Oxaliplatin, a potent inhibitor of survivin, enhances paclitaxel-induced apoptosis and mitotic catastrophe in colon cancer cells. *Jpn J. Clin. Oncol.* **35**, 453–463 (2005).
72. Uemura, R. et al. UVA-activated riboflavin promotes collagen crosslinking to prevent root caries. *Sci. Rep.* **9**, 1–11 (2019).
73. Wollensak, G., Spoerl, E. & Seiler, T. Riboflavin/ultraviolet-a-induced collagen crosslinking for the treatment of keratoconus. *Am. J. Ophthalmol.* **135**, 620–627 (2003).
74. Olde Damink, L. H. H. et al. Glutaraldehyde as a crosslinking agent for collagen-based biomaterials. *J. Mater. Sci. Mater. Med.* **6**, 460–472 (1995).
75. Lu, M., Song, X., Yang, M., Kong, W. & Zhu, J. Combined effects of glutaraldehyde and riboflavin/uv365 on the self-assembly of type I collagen molecules observed with atomic force microscopy. *Int. J. Food Prop.* **21**, 2181–2192 (2018).
76. Belin, M. W. et al. Corneal cross-linking: current USA status: report from the cornea society. *Cornea* **37**, 1218–1225 (2018).
77. Choi, M., Kim, J., Kim, E. K., Seo, K. Y. & Kim, T. I. Comparison of the conventional dresden protocol and accelerated protocol with higher ultraviolet intensity in corneal collagen cross-linking for keratoconus. *Cornea* **36**, 523–529 (2017).
78. Sheu, M.-T., Huang, J.-C., Yeh, G.-C. & Ho, H.-O. Characterization of collagen gel solutions and collagen matrices for cell culture. *Biomaterials* **22**, 1713–1719 (2001).
79. Legant, W. R. et al. Measurement of mechanical tractions exerted by cells in three-dimensional matrices. *Nat. Methods* **7**, 969–971 (2010).
80. Koenderink, G. H. et al. An active biopolymer network controlled by molecular motors. *Proc. Natl Acad. Sci. USA* **106**, 15192–15197 (2009).

81. Fernández-Castano Romera, M. et al. Mimicking active biopolymer networks with a synthetic hydrogel. *J. Am. Chem. Soc.* **141**, 1989–1997 (2019).
82. Sadasivuni, K. K. et al. Recent advances in mechanical properties of biopolymer composites: a review. *Polym. Compos.* **41**, 32–59 (2020).
83. Fan, A., Tofangchi, A., Kandel, M., Popescu, G. & Saif, T. Coupled circumferential and axial tension driven by actin and myosin influences in vivo axon diameter. *Sci. Rep.* **7**, 1–12 (2017).
84. Fan, A., Joy, M. S. H. & Saif, T. A connected cytoskeleton network generates axonal tension in embryonic: *Drosophila*. *Lab Chip* **19**, 3133–3139 (2019).
85. Wollensak, G., Spoerl, E. & Seiler, T. Riboflavin/ultraviolet-A-induced collagen crosslinking for the treatment of keratoconus. *Am. J. Ophthalmol.* **135**, 620–627 (2003).
86. Kohlhaas, M. et al. Biomechanical evidence of the distribution of cross-links in corneastreated with riboflavin and ultraviolet a light. *J. Cataract Refract. Surg.* **32**, 279–283 (2006).
87. Bersanetti, P. A. et al. Characterization of rabbit corneas subjected to stromal stiffening by the açaí extract (*Euterpe oleracea*). *Curr. Eye Res.* **42**, 528–533 (2017).
88. Wang, Z., Tang, Y., Tan, Y., Wei, Q. & Yu, W. Cancer-associated fibroblasts in radiotherapy: challenges and new opportunities. *Cell Commun. Signal.* **17**, 47 (2019).
89. Gorchs, L. et al. Cancer-associated fibroblasts from lung tumors maintain their immunosuppressive abilities after high-dose irradiation. *Front. Oncol.* **5**, 87 (2015).
90. Moffat, J. G., Vincent, F., Lee, J. A., Eder, J. & Prunotto, M. Opportunities and challenges in phenotypic drug discovery: an industry perspective. *Nat. Rev. Drug Discov.* **16**, 531–543 (2017).
91. Aulner, N., Danckaert, A., Ihm, J. E., Shum, D. & Shorte, S. L. Next-generation phenotypic screening in early drug discovery for infectious diseases. *Trends Parasitol.* **35**, 559–570 (2019).
92. Vincent, F. et al. Developing predictive assays: the phenotypic screening 'rule of 3. *Sci. Transl. Med.* **7**, 293ps15-293ps15 (2015).
93. Brown, D. G. & Wobst, H. J. Opportunities and challenges in phenotypic screening for neurodegenerative disease research. *J. Med. Chem.* **63**, 1823–1840 (2020).
94. Wang, E. Y., Zhao, Y., Okhovatian, S., Smith, J. B. & Radisic, M. Intersection of stem cell biology and engineering towards next generation in vitro models of human fibrosis. *Front. Bioeng. Biotechnol.* **10**, 963775 (2022).

Acknowledgements

Research reported in this publication was partially supported by the National Institute of Biomedical Imaging and Bioengineering of the National Institutes of Health under Award Number T32EB019944 to B.E. The content is solely the responsibility of the authors and does not necessarily represent the official views of the National Institutes of Health. Funding was also provided by the National Science Foundation grants ECCS 1934991 and CMMI 2342257, Mayo clinic grant PO 66236006 and Seed Grant from the Cancer Center at Illinois. M.T.A.S. is a CZ Biohub Investigator. We also thank the Paul Selvin lab for their assistance with the primary neurons, I. Choi for her assistance with PrCAFs, and A. Aly and J. Symanski for assistance with data analysis.

Author contributions

B.E. and M.T.A.S. conceived and designed the experiments. B.E., M.S.H.J. and W.C.D. performed the experiments, imaging and analysis. B.E., M.S.H.J., and M.T.A.S. prepared the manuscript. All authors have read and approved the final manuscript.

Competing interests

The authors declare no competing interests.

Additional information

Supplementary information The online version contains supplementary material available at https://doi.org/10.1038/s41596-024-01106-8.

Correspondence and requests for materials should be addressed to M. Taher A. Saif.

Peer review information *Nature Protocols* thanks Yun Chen, Huw Colin-York, Qiang Wei, and the other, anonymous, reviewer(s) for their contribution to the peer review of this work.